Absolute binding energies of electrons in condensed matters

- Four types of electronic excitations
- X-ray photoemission spectroscopy (XPS)
- Absolute binding energies of electrons
- Applications
- X-ray Absorption Near Edge Structure (XANES)
- Outlook

Taisuke Ozaki
Institute for Solid State Physics (ISSP)
Univ. of Tokyo

Second Workshop on Fundamentals in density functional theory (DFT2024) in Kobe, Feb. 20th, 2024.

Four types of electronic excitations

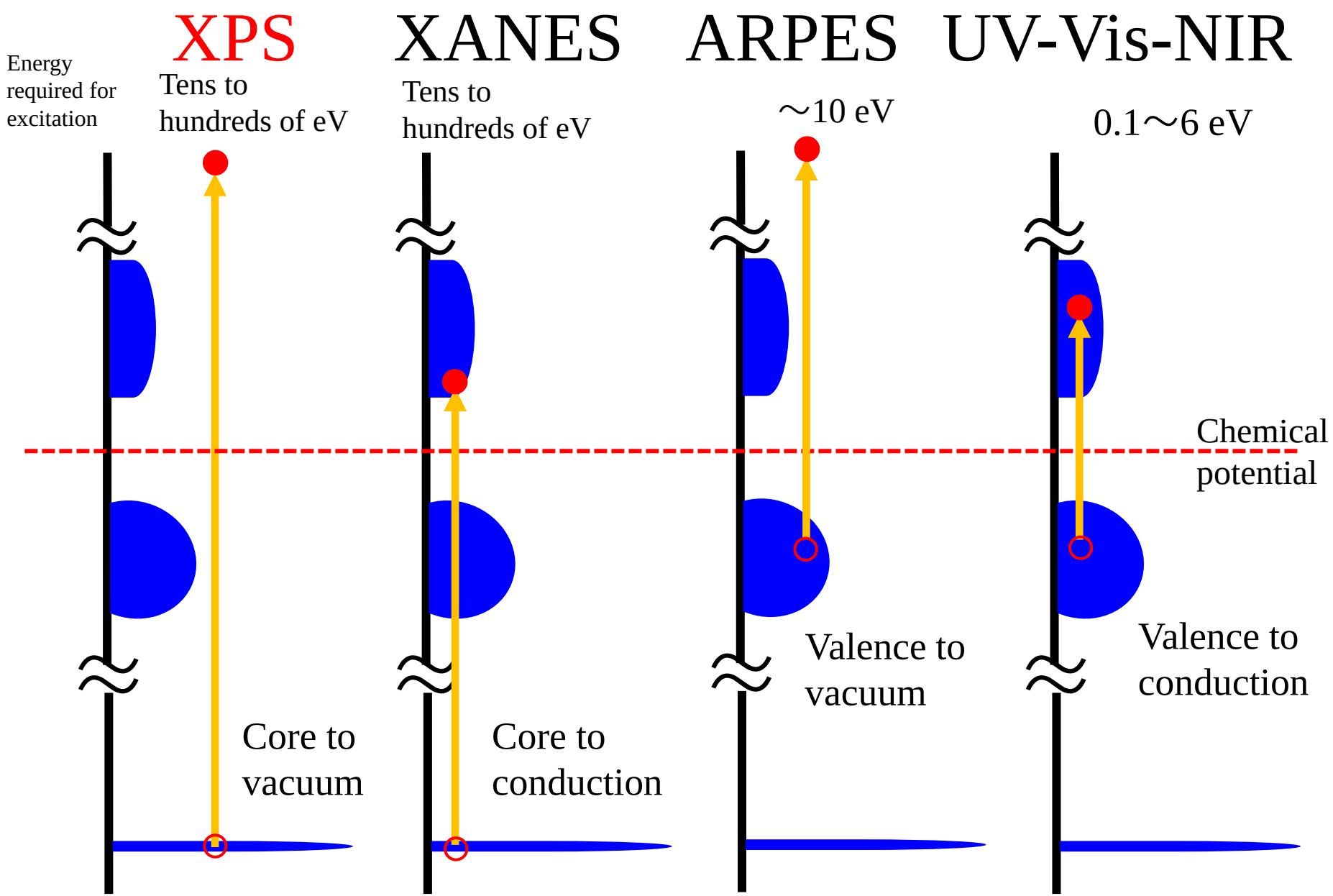

X-ray photoemission spectroscopy (XPS)

- X-ray photoelectron spectroscopy (XPS) is a general technique for analyzing composition, surface structure, and adsorbents on surfaces.
- XPS with synchrotron radiation extends its usefulness, e.g., satellite analysis, core level vibrational fine structure, XPS circular dichroism, spin-resolved XPS, and XPS holography.

Holography image of atomic positions under Cu(001) surface

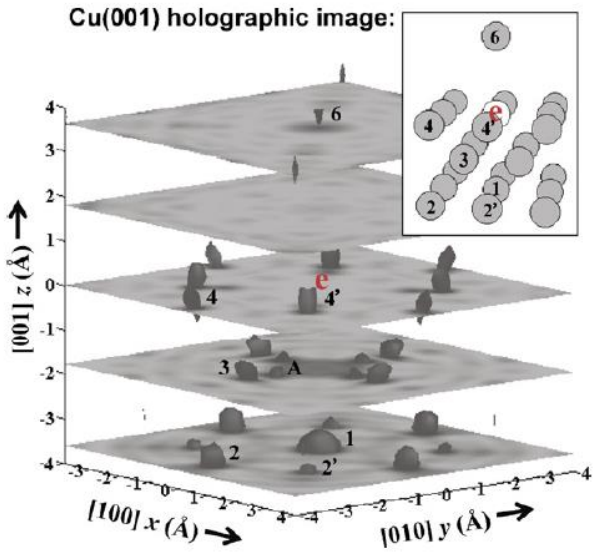

S. Omori et al., PRL 88, 5504 (2002).

Magnetic circular dichroism of Fe layer on Cr substrate

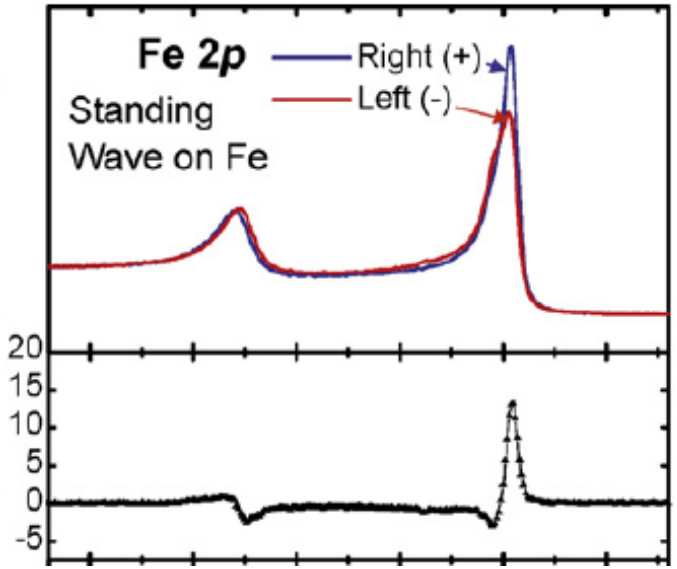

S.-H. Yang et al., J. Phys. Condens. Matter 14, L407 (2002).

XPS experiments

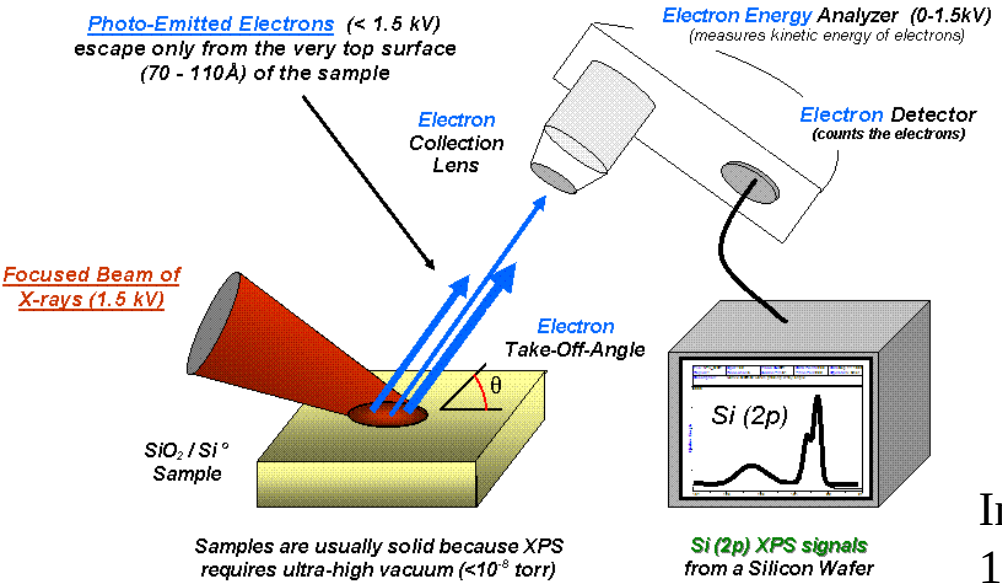

https://en.wikipedia.org/wiki/X-ray_photoelectron_spectroscopy

Appearance of XPS equipment

In general, XPS requires high vacuum (P ~ 10^{-8} millibar) or ultra-high vacuum (UHV; P < 10^{-9} millibar) conditions.

Surface sensitivity: Inelastic Mean Free Path (IMFP)

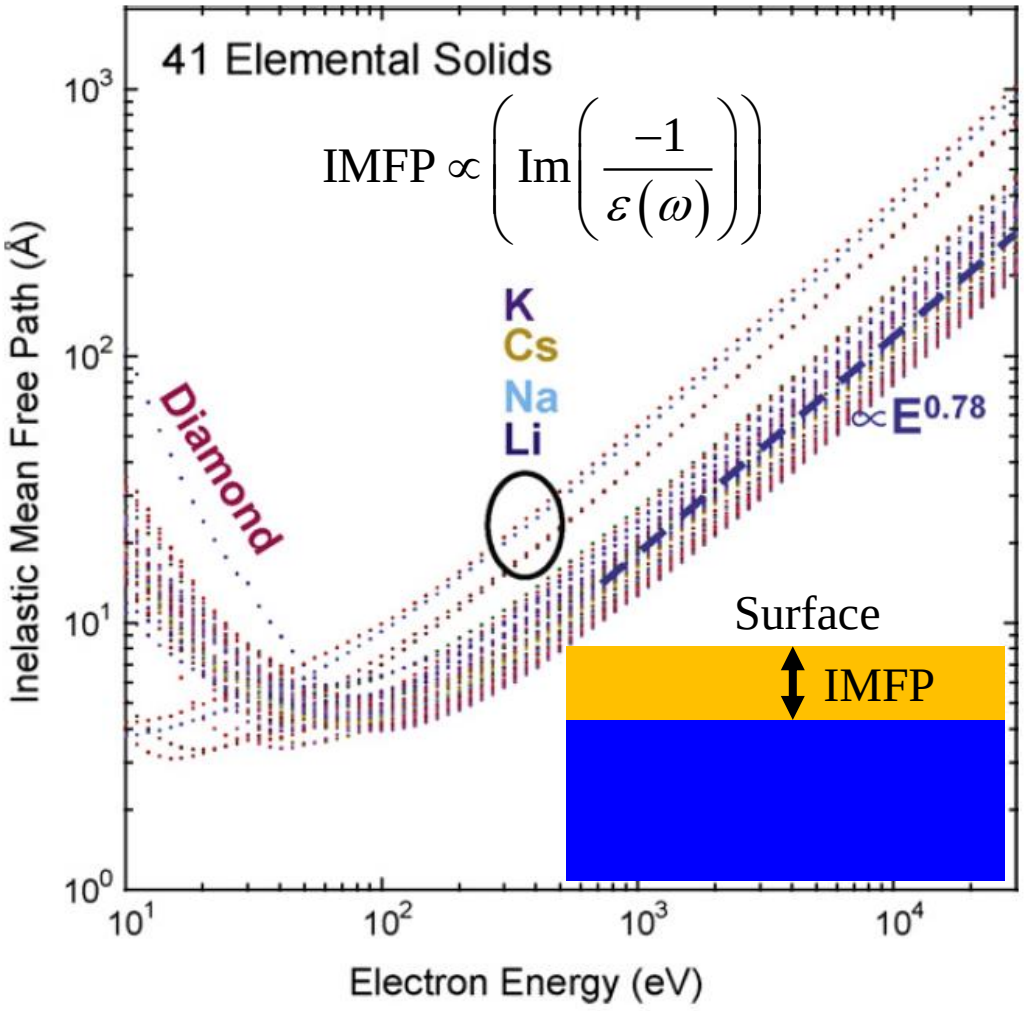

C.S. Fadley, Journal of Electron Spectroscopy and Related Phenomena 178-179, 2 (2010).

Fig. 2. Inelastic mean free paths (IMFPs) for 41 elements, calculated using the TPP-2M formula: Li, Be, three forms of carbon (graphite, diamond, glassy C), Na, Mg, Al, Si, K, Sc, Ti, V, Cr, Fe, Co, Ni, Cu, Ge, Y, Nb, Mo, Ru, Rh, Pd, Ag, In, Sn, Cs, Gd, Tb, Dy, Hf, Ta, W, Re, Os, Ir, Pt, Au, and Bi. Five "outlier" elements are indicated to provide some idea of what electronic structure characteristics can give rise to deviations from the majority behavior: diamond and the alkali metals. The dashed straight line for higher energies represents a variation as $\Lambda_e \propto E_{kin}^{0.78}$, and is a reasonable first approximation to the variation for all of the elements shown (from Ref. [23]).

- Inelastic Mean Free Path (IMFP) of photo excited electron for 41 elemental solids is shown the left figure.
- In case of the widely used aluminum K-alpha X-ray having 1486.7 eV, the IMFP is found to be 15 ~ 100 Å.
- On the other hand, when X-rays generated by synchrotron radiation is utilized, which have energy up to 15 keV, the IMFP can be more than 100 Å.

Element specific measurement

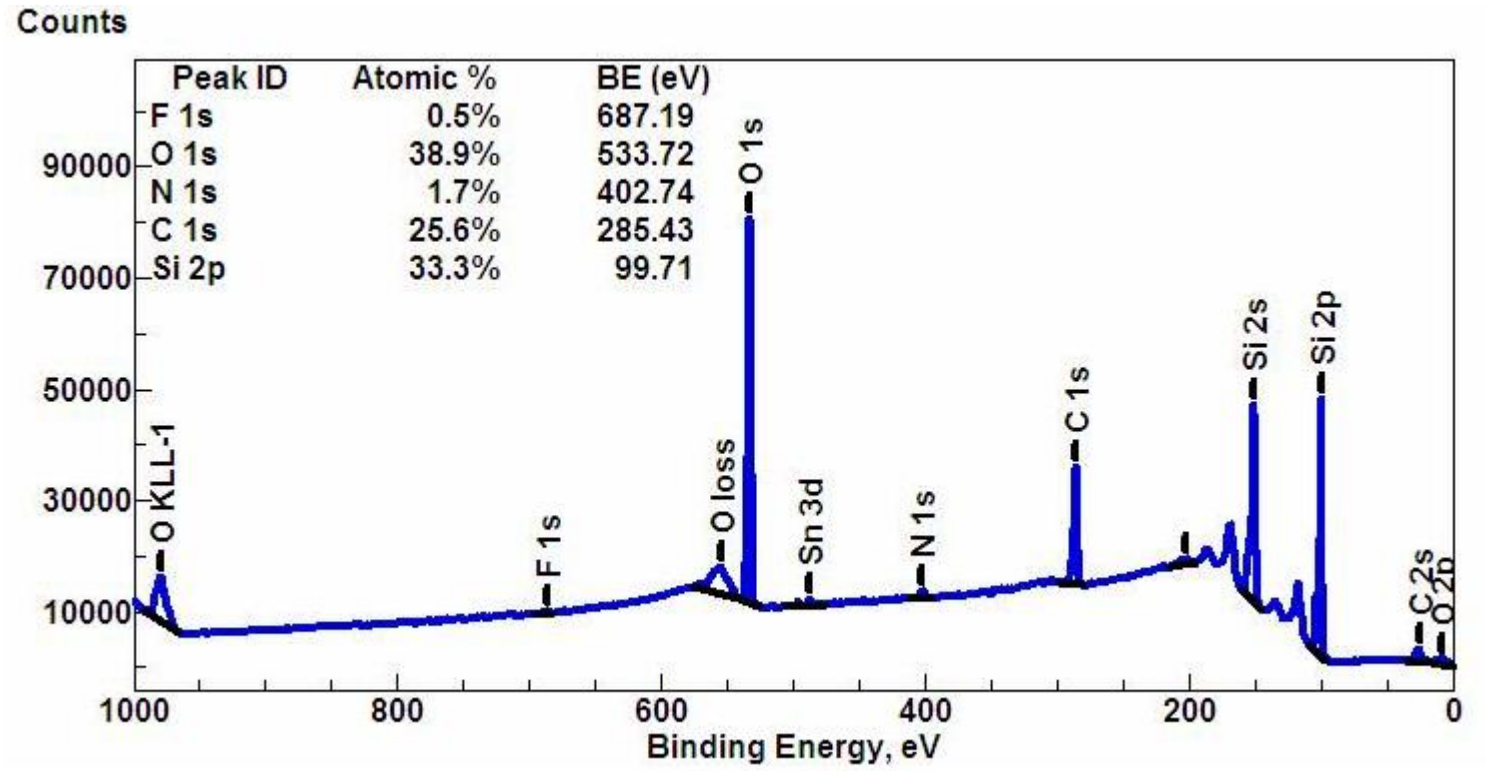

- The binding energy of each core level in each element is specific, and by this reason one can identify element and composition in a material under investigation by a wide scan mode, while hydrogen and helium cannot be identified because of low binding energies overlapping to other valence states.

- The database which is a huge collection of experimental data measured by XPS is available at http://srdata.nist.gov/xps/Default.aspx

https://en.wikipedia.org/wiki/X-ray_photoelectron_spectroscopy

Basic physics in X-ray photoelectron spectroscopy (XPS)

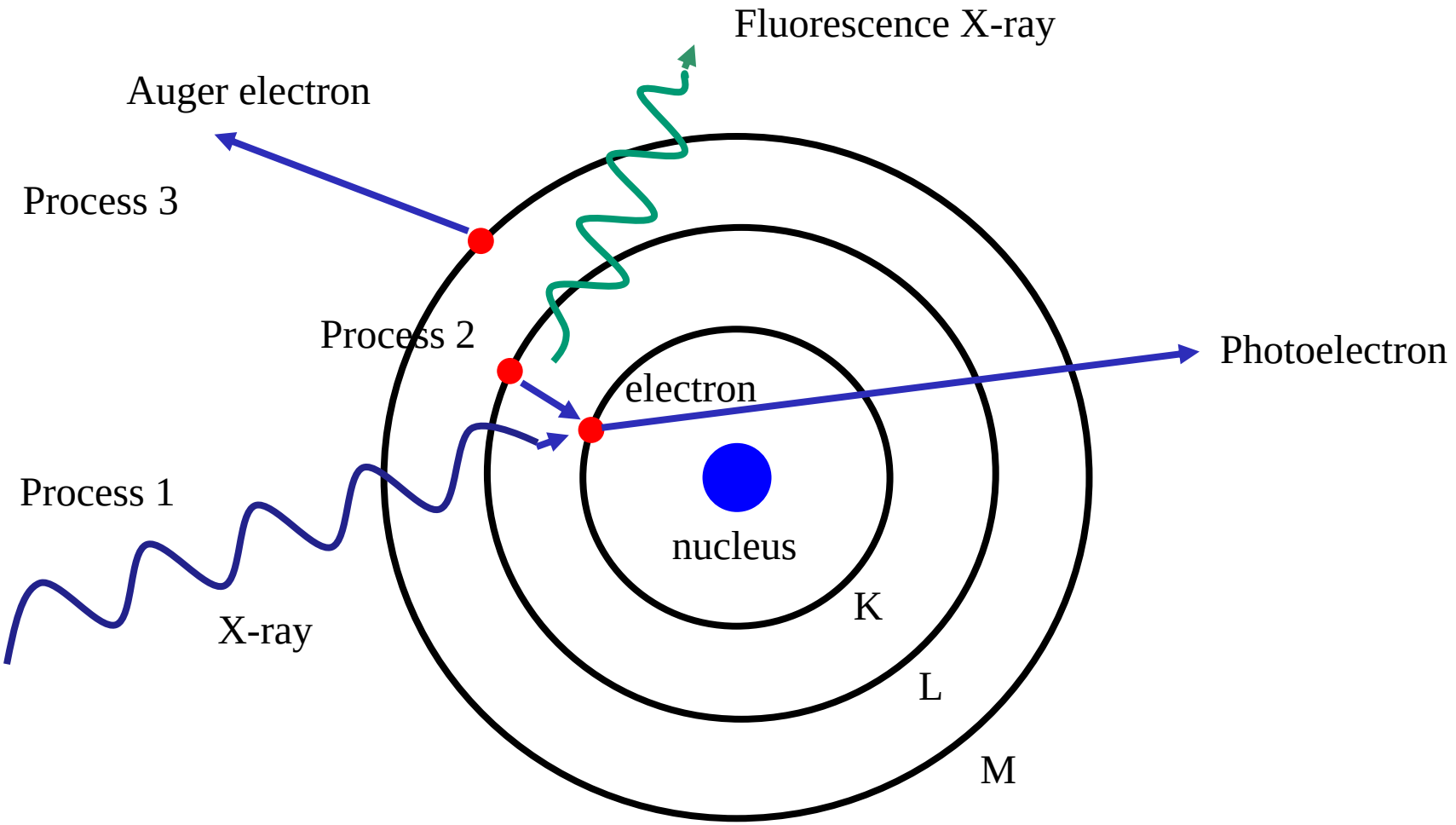

Escape time of photoelectron seems to be considered around 10^{-16} sec., resulting in relaxation of atomic structure would be ignored.

Physical origins of multiple splitting in XPS

The absolute binding energies of core electrons in solids split due to the following intrinsic physical origins:

- Chemical shift (chemical environment)
- Spin-orbit splitting
- Magnetic exchange interaction
- Chemical potential shift

T. Ozaki and C.-C. Lee, Phys. Rev. Lett. 118, 026401 (2017).

Chemical environment

- The binding energy shifts depending on its chemical environment. The amount of shift is primary determined by its charge state, known to be **initial state effect**.
- After creating the core hole, the screening of the core hole is also an important factor to determine chemical shift, known to be **final state effect**.

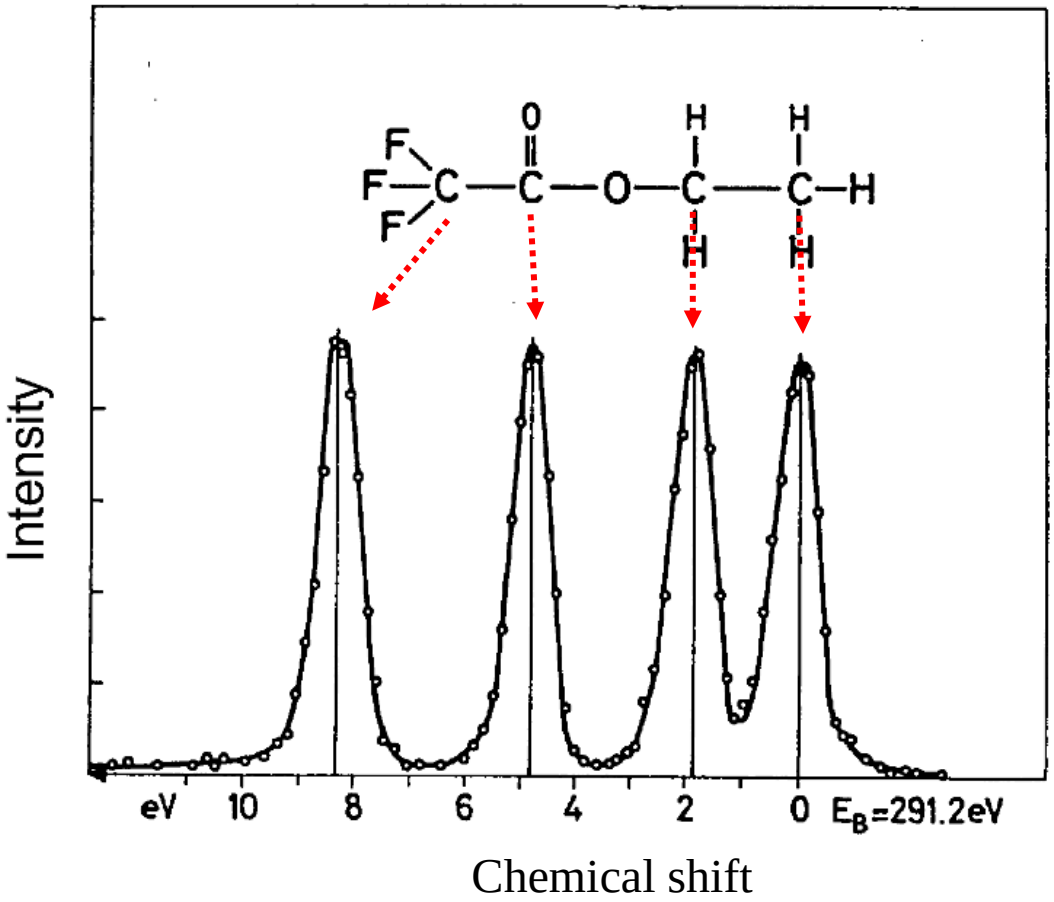

"PHOTOEMISSION SPECTROSCOPY Fundamental Aspects" by Giovanni Stefani

Spin-orbit splitting

In addition to the chemical shift, there are other multiplet splittings.

Spin-orbit coupling of core level

- Due to the strong SOC of core level states, the binding energy is split into two levels.
- The intensity ratio is 2l: 2(l+1) for l-1/2 and l+1/2, respectively.

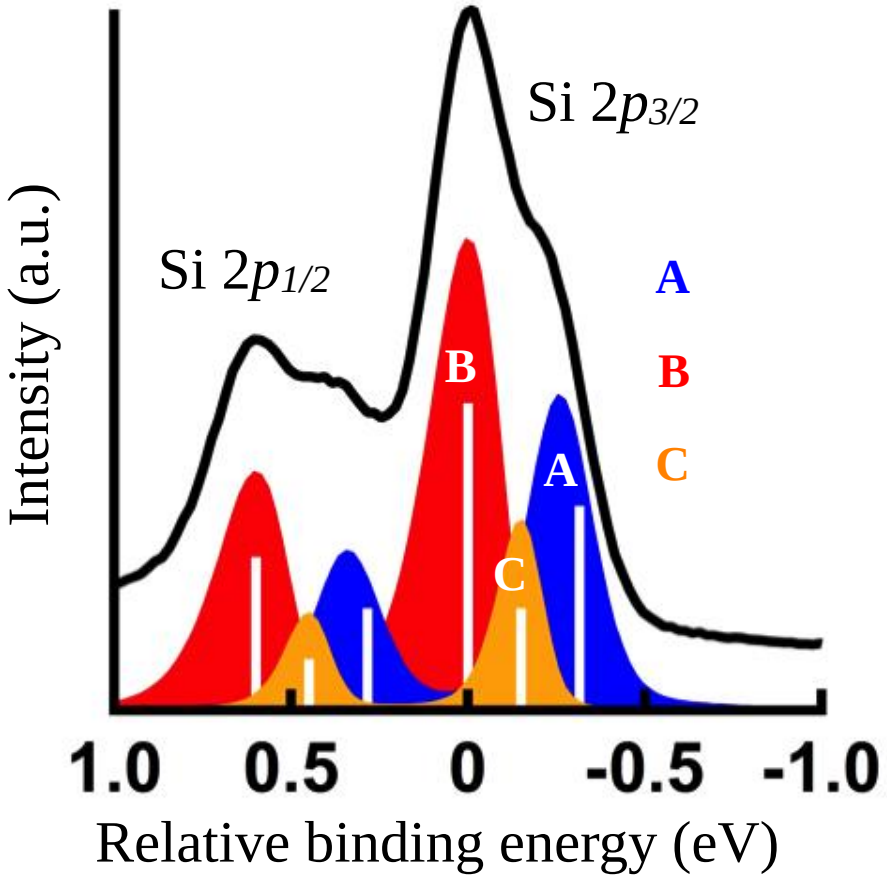

A. Fleurence et al., PRL 108, 245501 (2012).

Silicene on ZrB_2 surface

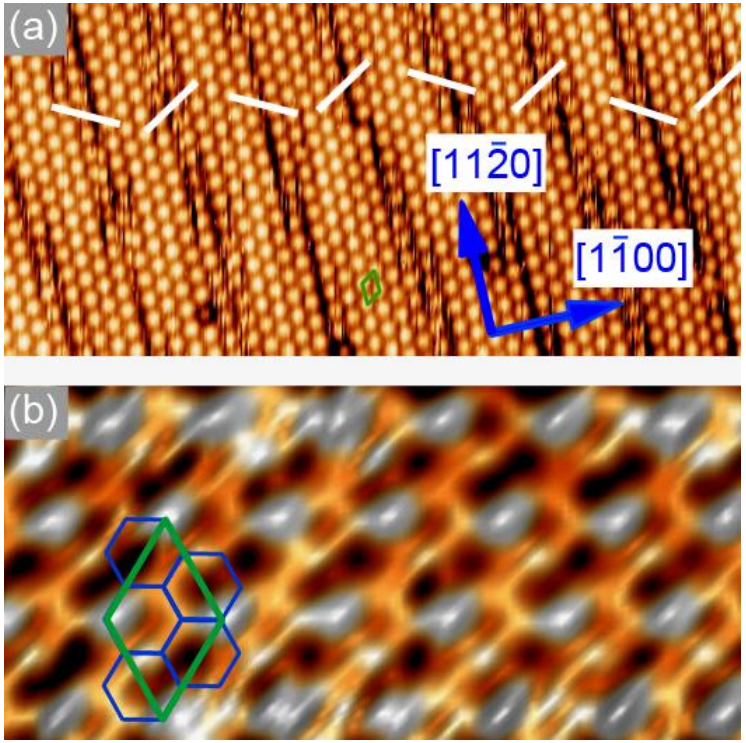

Core level multiple splitting: Exchange interaction

Exchange interaction between core and valence electrons

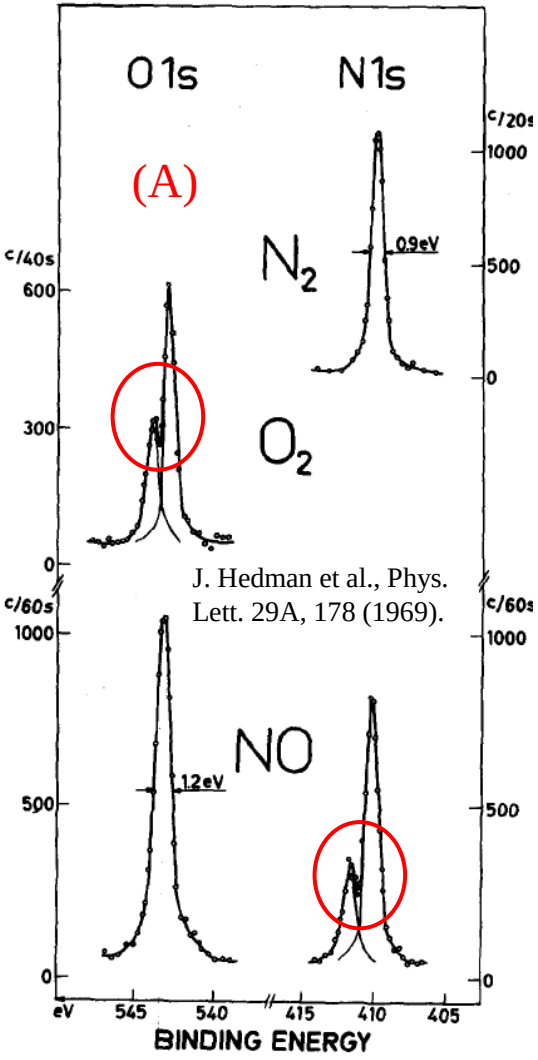

J. Hedman et al., Phys. Lett. 29A, 178 (1969).

Fig. 1. ESCA spectra of core electron levels in N_2, O_2, and NO. Paramagnetic splitting is observed for the 1s levels in the O_2 and NO molecules.

- After creation of core hole, the remaining core electron is spin polarized.
- If the valence electron is spin polarized in the initial state, there must be an exchange interaction between the remaining core electron and valence electrons even in the final state.
- The exchange interaction results in multiplet splitting.

- The left figure (A) shows that the 1s binding energy of oxygen and nitrogen atom splits in magnetic molecules O_2 and NO, respectively, while no splitting is observed in N_2 being a non-magnetic molecule.
- The right figure (B) shows the splitting of 3s binding energy of Mn atom in manganese compounds.

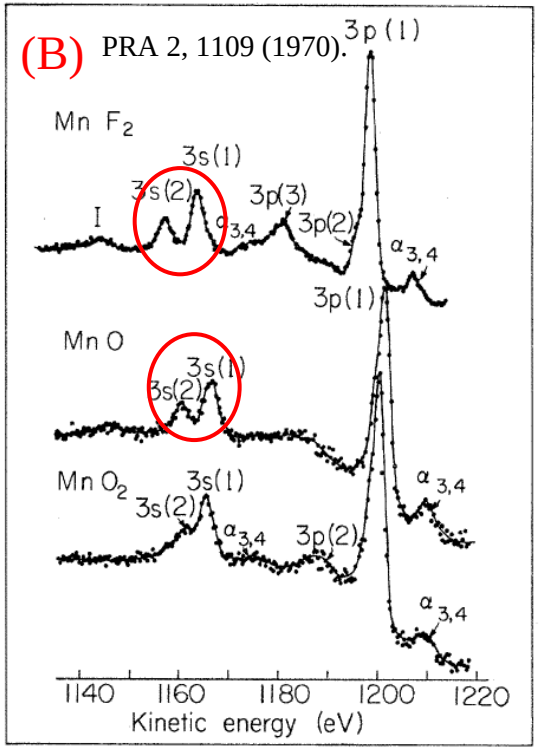

FIG. 1. Photoelectron spectra from MnF_2, MnO, and MnO_2 in the kinetic-energy region corresponding to ejection of Mn 3s and 3p electrons by Mg $K\alpha$ x rays.

Shift of chemical potential in semi-conductors and insulators

The chemical potential in gapped systems varies sensitively depending on impurity, vacancy, surface structures, and adsorbate.

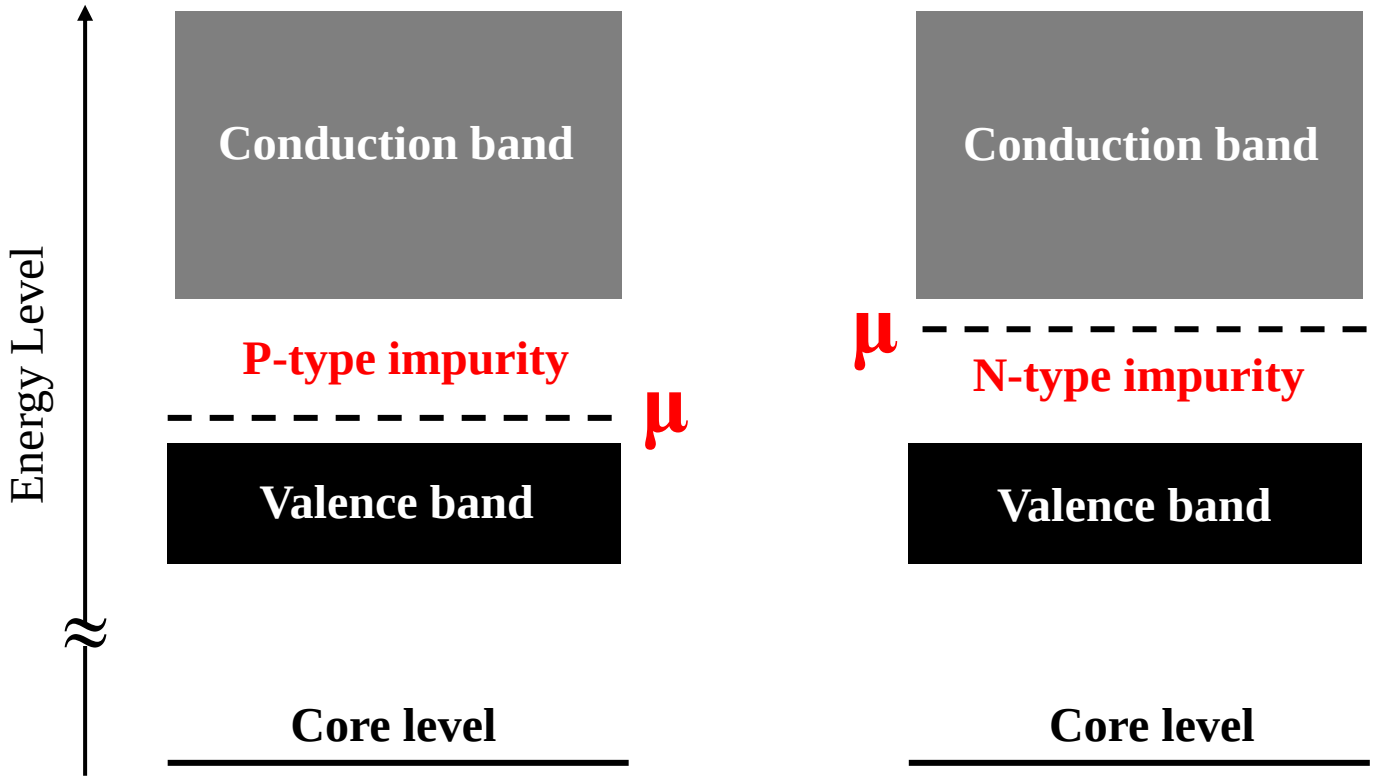

Severely speaking, we need to take account of the effect explicitly by considering realistic models which reflect experimental situations.

Energy conservation in XPS

$$E_i(N) + h\nu = E_f(N-1) + V_{spec} + K_{spec}$$

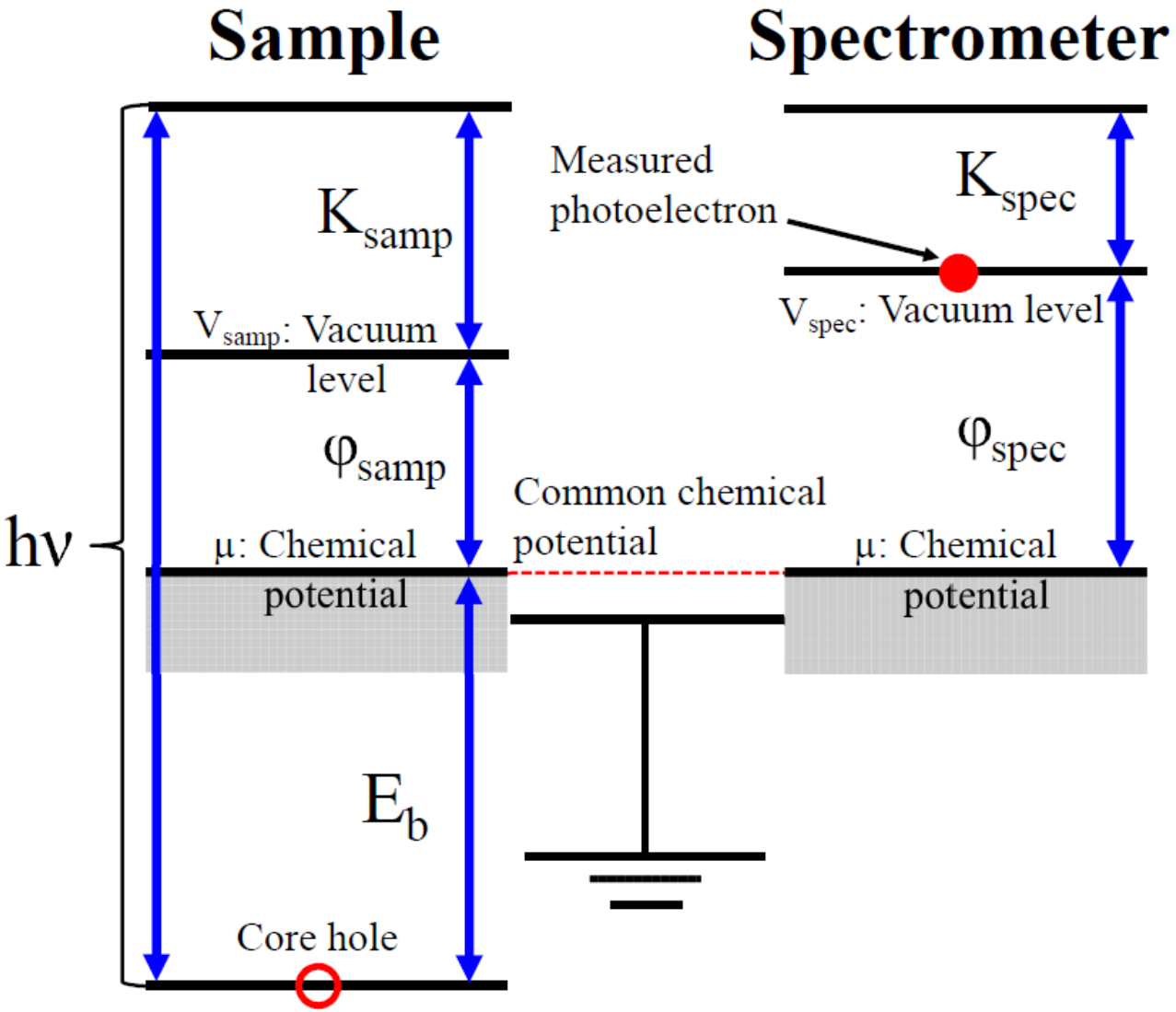

Core level binding energies in XPS #1

$$E_{\mathrm{i}}(N)+h\nu = E_{\mathrm{f}}(N-1)+V_{\mathrm{spec}}+K_{\mathrm{spec}}$$

Using a relation: $V_{\mathrm{spec}} = \mu + \varphi_{\mathrm{spec}}$ we have

$$E_{\mathrm{b}} = h\nu - K_{\mathrm{spec}} - \phi_{\mathrm{spec}} = E_{\mathrm{f}}(N-1) - E_{\mathrm{i}}(N) + \mu$$

The experimental chemical potential can be transformed as

$$E_{\mathrm{b}} = E_{\mathrm{f}}^{(0)}(N-1)+(N-1)\Delta\mu - \left(E_{\mathrm{i}}^{(0)}(N)+N\Delta\mu\right)+\mu_0+\Delta\mu$$

A general formula of core level binding is given by

$$E_{\mathrm{b}} = E_{\mathrm{f}}^{(0)}(N-1) - E_{\mathrm{i}}^{(0)}(N) + \mu_0$$

This is common for metals and insulators.

Core level binding energies in XPS #2

For metals, the Janak theorem simplifies the formula:

$$E_{\mathrm{f}}^{(0)}(N-1) - E_{\mathrm{f}}^{(0)}(N) = \int dn \partial E_{\mathrm{f}}^{(0)} / \partial n = -\mu_0$$

$$E_{\mathrm{b}} = E_{\mathrm{f}}^{(0)}(N) - E_{\mathrm{i}}^{(0)}(N)$$

The formulae of core level binding energies are summarized as

Solids (gapped systems, metals) $E_{\mathrm{b}} = E_{\mathrm{f}}^{(0)}(N-1) - E_{\mathrm{i}}^{(0)}(N) + \mu_0$

Metals $E_{\mathrm{b}} = E_{\mathrm{f}}^{(0)}(N) - E_{\mathrm{i}}^{(0)}(N)$

Gases $E_{\mathrm{b}} = E_{\mathrm{f}}^{(0)}(N-1) - E_{\mathrm{i}}^{(0)}(N)$

Calculations: core level binding energy

Within DFT, there are at least three ways to calculate the binding energies of core states as summarized below:

1. **Initial state theory**

   Simply the density of states is taken into account

2. **Core-hole pseudopotential method**

   Full initial and semi-final state effects are taken into account

   E. Pehlke and M. Scheffler, PRL 71 2338 (1993).

3. **Core-hole SCF method**

   The initial and final state effects are fully taken into account on the same footing.

   T. Ozaki and C.-C. Lee, Phys. Rev. Lett. 118, 026401 (2017) .

Density functional theory (DFT)

- The ground state total energy can be described as density functional.

  Hohenberg-Kohn theorem

$$E[\rho] = \int dr^3 \rho(\mathbf{r}) v_{\text{ext}}(\mathbf{r}) + T[\rho] + J[\rho] + E_{\text{xc}}[\rho]$$

- By including quantum mechanical many-body effects in the exchange-correlation energy, the many-body problem can be formulated as an one-body problem.

  Kohn-Sham method

$$\hat{H}_{\text{KS}}\phi_i = \varepsilon_i \phi_i \qquad \hat{H}_{\text{KS}} = -\frac{1}{2}\nabla^2 + v_{\text{eff}}$$

$$v_{\text{eff}}(\mathbf{r}) = v_{\text{ext}}(\mathbf{r}) + v_{\text{Hartree}}(\mathbf{r}) + \frac{\delta E_{xc}}{\delta \rho(\mathbf{r})}$$

Gunnarsson-Lundqvist theorem

(1) Many body Schrodinger equation:

$$\hat{H}\Psi_i = E_i \Psi_i$$

(2) We classify WFs to two classes.

$$\{\Psi\} \rightarrow \{\Psi^{(A)}\}, \{\Psi^{(B)}\}$$

$$\hat{O}\Psi_i^{(A)} = \lambda^{(A)}\Psi_i^{(A)}$$

Class A: $\lambda^{(A)}$
Class B: non $\lambda^{(A)}$

$$\hat{O}\Psi_i^{(B)} = \lambda_i^{(B)}\Psi_i^{(B)}$$

(3) Define the projector operator:

$$\hat{A} = \Delta\left(\hat{1} - \sum_{i\in A} \left|\Psi_i^{(A)}\right\rangle\left\langle\Psi_i^{(A)}\right|\right)$$

(4) A new Hamiltonian is given by

$$\hat{H}_A = \hat{H} + \hat{A}$$

(5) By minimizing the expectation value of $\hat{H}_A$, we find the lowest state within the class A.

$$\min_{\Psi} \frac{\langle\Psi|\hat{H}_A|\Psi\rangle}{\langle\Psi|\Psi\rangle} \Rightarrow E_{\min}^{(A)}$$

Gunnarsson and Lundqvist, PRB 13, 4274 (1976).

Excited states with a core hole

$$\hat{H}\Psi_i = E_i\Psi_i$$

$\{\Psi\}$ → $\{\Psi^{(A)}\}$ States with a core hole on a targeted atom

$\{\Psi^{(B)}\}$ No core hole

For our purpose, we can choose the following projector:

$$\hat{O} = 1 - \hat{a}_c^\dagger \hat{a}_c = 1 - \hat{n}_c$$

Then, we have

$$(1-\hat{n}_c)\left|\Psi^{(A)}\right\rangle = \left|\Psi^{(A)}\right\rangle$$

$$(1-\hat{n}_c)\left|\Psi^{(B)}\right\rangle = 0$$

Thus, it turns out that the Gunnarsson-Lundqvist theorem is valid for the core excitation problems.

Levy's two-step minimization for $\hat{\mathrm{H}}_{\mathrm{A}}$

We apply the Levy's two-step minimization for $\hat{\mathrm{H}}_{\mathrm{A}}$.

$$
\begin{aligned}
E &= \min_{\Psi} \left\langle \Psi \middle| \hat{\mathrm{H}}_{\mathrm{A}} \middle| \Psi \right\rangle \\
&= \min_{\rho} \left(\min_{\Psi \to \rho} \left\langle \Psi \middle| \hat{\mathrm{H}}_{\mathrm{A}} \middle| \Psi \right\rangle \right) \qquad \text{Choose N-representable } \rho \\
&= \min_{\rho} \left(\min_{\Psi \to \rho} \left[\left\langle \Psi \middle| \left(\hat{T} + \hat{v}_{\mathrm{ee}} \right) \middle| \Psi \right\rangle + \left\langle \Psi \middle| \hat{\mathrm{A}} \middle| \Psi \right\rangle \right] + \int v(\mathbf{r}) \rho(\mathbf{r}) d\mathbf{r} \right) \\
&= \min_{\rho} \left(F_{\mathrm{A}} \left[\rho \right] + \int v(\mathbf{r}) \rho(\mathbf{r}) d\mathbf{r} \right)
\end{aligned}
$$

- It turns out that DFT can be applied for $\hat{\mathrm{H}}_{\mathrm{A}}$.
- The functional F is dependent of A.
- By choosing states with a core hole as the class A, one can treat core level excitation spectra such as XPS and XANES.

What we noticed

- The Gunnarsson-Lundqvist theorem allows us to calculate the lowest excited state with a given symmetry of wave function.
- Thus, the total energy of the lowest excited state with a core hole can be rigorously calculated by DFT in principle.
- Since the XPS requires only the lowest excited state with (N-1) electrons, DFT must provide an accurate framework to calculate the core level binding energy.
- For the other spectroscopies including XANES, XMCD, and EELS, the lowest excitation must be calculated accurately, but higher excited states will be treated approximately.

Kohn-Sham system for the lowest excited state with a core hole

$$E_{\mathrm{CH}} = T_{\mathrm{s}} + E_{\mathrm{ec}} + E_{\mathrm{Hart}} + E_{\mathrm{xc}}^{(\mathrm{CH})} + E_{\mathrm{cc}}$$

Noting that the functional F_{A} in the Levy's constraint minimization is related to the energy terms in the KS total energy by

$$F_{\mathrm{A}} = \min_{\Psi\to\rho}\left[\left\langle\Psi\middle|\left(\hat{T}+\hat{v}_{\mathrm{ee}}\right)\middle|\Psi\right\rangle + \left\langle\Psi\middle|\hat{\mathrm{A}}\middle|\Psi\right\rangle\right] = T_{\mathrm{s}} + E_{\mathrm{Hart}} + E_{\mathrm{xc}}^{(0)} + T - T_{\mathrm{s}}$$
$$= T_{\mathrm{s}} + E_{\mathrm{Hart}} + E_{\mathrm{xc}}^{(\mathrm{CH})}$$

and considering the role of the projection operator $\hat{\mathrm{A}}$, we may be able to approximate the exchange-correlation term as

$$E_{\mathrm{xc}}^{(\mathrm{CH})} = E_{\mathrm{xc}}^{(\mathrm{G})} + E_{\mathrm{p}}$$

$E_{\mathrm{xc}}^{(\mathrm{G})}$ Functional for ground state

E_{p} Penalty functional

Core hole dependent E_{xc}

The penalty functional we use is given by

R: radial function of the core level
Δ: large positive number

$$E_{\mathrm{p}} = \langle \Psi^{(\mathrm{CH})} \mid \hat{P} \mid \Psi^{(\mathrm{CH})} \rangle \qquad \hat{P} = \left| R\Phi_J^M \right\rangle \Delta \left\langle R\Phi_J^M \right|$$

The projector is given by a solution of Dirac eq. for atoms.

$$J = l + \frac{1}{2}, M = m + \frac{1}{2}$$

$$|\Phi_J^M\rangle = \left(\frac{l+m+1}{2l+1}\right)^{\frac{1}{2}} |Y_l^m\rangle + \left(\frac{l-m}{2l+1}\right)^{\frac{1}{2}} |Y_l^{m+1}\rangle$$

$$J = l - \frac{1}{2}, M = m - \frac{1}{2}$$

$$|\Phi_J^M\rangle = \left(\frac{l-m+1}{2l+1}\right)^{\frac{1}{2}} |Y_l^{m-1}\rangle + \left(\frac{l+m}{2l+1}\right)^{\frac{1}{2}} |Y_l^m\rangle$$

Since it is expected that the quantum fluctuation for the core hole state in ψ is expected to be small, one can approximate as

$$E_{\mathrm{p}} = \langle \Psi^{(\mathrm{CH})} \mid \hat{P} \mid \Psi^{(\mathrm{CH})} \rangle \simeq \langle \Phi^{(\mathrm{CH})} \mid \hat{P} \mid \Phi^{(\mathrm{CH})} \rangle$$

$\Phi^{(\mathrm{CH})}$
KS Slater determinant with a core hole

Thus, we have

$$E_{\mathrm{p}} = \frac{1}{V_{\mathrm{B}}} \int dk^3 \sum_{\mu} f_{\mu}^{(\mathbf{k})} \langle \varphi_{\mu}^{(\mathbf{k})} \mid \hat{P} \mid \varphi_{\mu}^{(\mathbf{k})} \rangle$$

Kohn-Sham eq. with a penalty operator

By variationally differentiating the penalty functional E_f, we obtain the following the KS equation.

$$\left(\hat{T} + V_{\text{eff}} + \hat{P}\right)|\psi_{\mu}^{(\mathbf{k})}\rangle = \varepsilon_{\mu}^{(\mathbf{k})}\,|\psi_{\mu}^{(\mathbf{k})}\rangle$$

Features of the method

- applicable to insulators and metals
- accessible to absolute binding energies
- screening of core and valence electrons on the same footing
- SCF treatment of spin-orbit coupling
- exchange interaction between core and valence states
- geometry optimization with a core hole state

Relativistic pseudopotentials

By using the eigenfunctions of the spherical operator for the Dirac Eq., one can introduce a relativistic pseudopotential as

$$V^{(\mathrm{ps})} = v^{(\mathrm{L})} + \hat{v}^{(\mathrm{NL})}_{l+\frac{1}{2}} + \hat{v}^{(\mathrm{NL})}_{l-\frac{1}{2}}$$

$$\hat{v}^{(\mathrm{NL})}_{l+\frac{1}{2}} = \sum_{lm}\sum_{\zeta} |v^{(\mathrm{NL})}_{l+\frac{1}{2}} \bar{R}_{J\zeta}\Phi^{M}_{J}\rangle \frac{1}{c_{J\zeta}} \langle \bar{R}_{J\zeta}\Phi^{M}_{J} v^{(\mathrm{NL})}_{l+\frac{1}{2}}|,$$

$$\hat{v}^{(\mathrm{NL})}_{l-\frac{1}{2}} = \sum_{lm}\sum_{\zeta} |v^{(\mathrm{NL})}_{l-\frac{1}{2}} \bar{R}_{J'\zeta}\Phi^{M'}_{J'}\rangle \frac{1}{c_{J'\zeta}} \langle \bar{R}_{J'\zeta}\Phi^{M'}_{J'} v^{(\mathrm{NL})}_{l-\frac{1}{2}}|.$$

for $J = l + \frac{1}{2}$ and $M = m + \frac{1}{2}$

$$|\Phi^{M}_{J}\rangle = \left(\frac{l+m+1}{2l+1}\right)^{\frac{1}{2}} |Y^{m}_{l}\rangle|\alpha\rangle + \left(\frac{l-m}{2l+1}\right)^{\frac{1}{2}} |Y^{m+1}_{l}\rangle|\beta\rangle,$$

for $J' = l - \frac{1}{2}$ and $M' = m - \frac{1}{2}$

$$|\Phi^{M'}_{J'}\rangle = \left(\frac{l-m+1}{2l+1}\right)^{\frac{1}{2}} |Y^{m-1}_{l}\rangle|\alpha\rangle - \left(\frac{l+m}{2l+1}\right)^{\frac{1}{2}} |Y^{m}_{l}\rangle|\beta\rangle.$$

Elimination of inter-core hole interaction

$$\rho_{\mathrm{f}}(\mathbf{r}) = \rho_{\mathrm{i}}(\mathbf{r}) + \Delta\rho(\mathbf{r}) \qquad \Delta\rho(\mathbf{r}) = \rho_f(\mathbf{r}) - \rho_i(\mathbf{r})$$

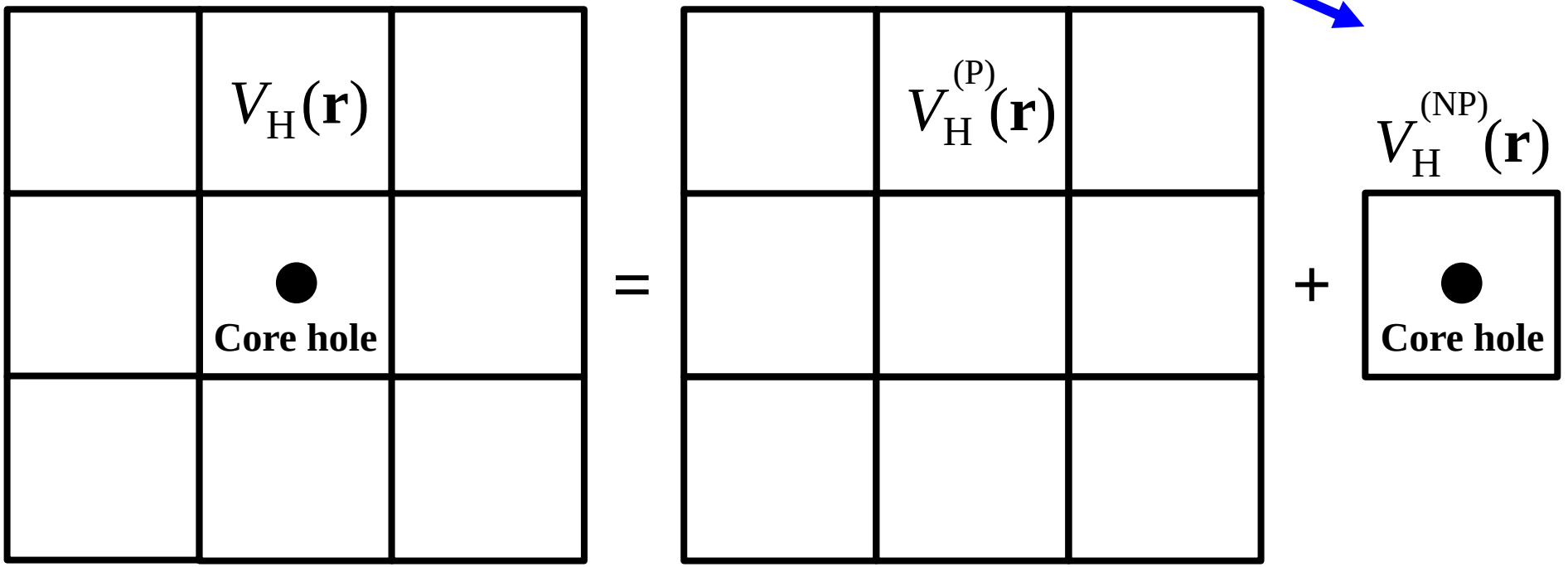

- Periodic Hartree potential is calculated by charge density of the initial state.
- Potential by induced charge is calculated by an exact Coulomb cutoff method.

Exact Coulomb cutoff method #1

If the charge induced by a core hole localizes within a radius of R, we can set R_c=2R, and the cutoff condition becomes $2R_c$<L to eliminate the inter-core hole interaction.

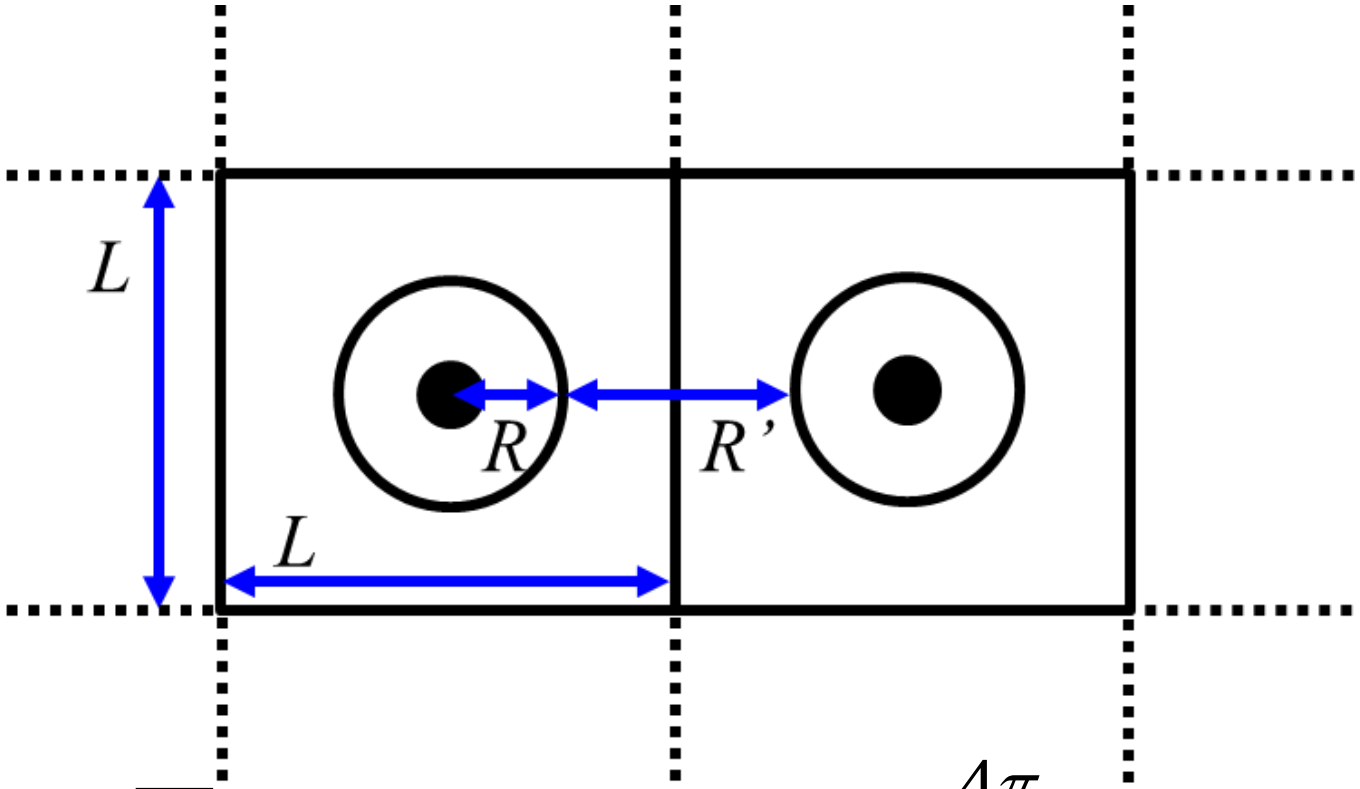

$$v_{\mathrm{H}}(r) = \sum_{\mathbf{G}} \tilde{n}(\mathbf{G})\tilde{v}(\mathbf{G})\mathrm{e}^{i\mathbf{G}\bullet r} \qquad \tilde{v}(\mathbf{G}) = \frac{4\pi}{G^2}(1-\cos GR_{\mathrm{c}})$$

Jarvis et al., PRB 56, 14972 (1997).

Exact Coulomb cutoff #2

$$v_{\mathrm{H}}(r) = \int dr' n(r') v(|r - r'|) \quad \cdots(1)$$

$$n(r) = \sum_{\mathbf{G}} \tilde{n}(\mathbf{G})\, \mathrm{e}^{i\mathbf{G}\bullet r} \quad \cdots(2) \qquad v(r) = \sum_{\mathbf{G}} \tilde{v}(\mathbf{G})\, \mathrm{e}^{i\mathbf{G}\bullet r} \quad \cdots(3)$$

By inserting (2) and (3) into (1), and performing the integration, we obtain

$$v_{\mathrm{H}}(r) = \sum_{\mathbf{G}} \tilde{n}(\mathbf{G}) \tilde{v}(\mathbf{G}) \mathrm{e}^{i\mathbf{G}\bullet r}$$

$\tilde{v}(\mathbf{G})$ is evaluated by performing the integration as

$$v(r) = \frac{1}{r} \quad \text{if } r <= R_c \qquad \tilde{v}(\mathbf{G}) = \int_0^{R_c} dr r^2 \int_0^{2\pi} d\phi \int_0^{\pi} d\theta \sin\theta \frac{\mathrm{e}^{i\mathbf{G}\bullet\mathbf{r}}}{r}$$

$$v(r) = 0 \quad \text{if } R_c < r \qquad \tilde{v}(\mathbf{G}) = \frac{4\pi}{G^2}(1 - \cos GR_c)$$

C.A. Rozzi et al., PRB 73, 205119.

OpenMX Open source package for Material eXplorer

https://www.openmx-square.org/

- Software package for density functional calculations of molecules and bulks
- Norm-conserving pseudopotentials (PPs)
- Variationally optimized numerical atomic basis functions

Basic functionalities

- SCF calc. by LDA, GGA, DFT+U
- Total energy and forces on atoms
- Band dispersion and density of states
- Geometry optimization by BFGS, RF, EF
- Charge analysis by Mullken, Voronoi, ESP
- Molecular dynamics with NEV and NVT ensembles
- Charge doping
- Fermi surface
- Analysis of charge, spin, potentials by cube files
- Database of optimized PPs and basis funcitons

Extensions

- O(N) and low-order scaling diagonalization
- Non-collinear DFT for non-collinear magnetism
- Spin-orbit coupling included self-consistently
- Electronic transport by non-equilibrium Green function
- Electronic polarization by the Berry phase formalism
- Maximally localized Wannier functions
- Effective screening medium method for biased system
- Reaction path search by the NEB method
- Band unfolding method
- STM image by the Tersoff-Hamann method
- etc.

Convergence w. r. t cell size

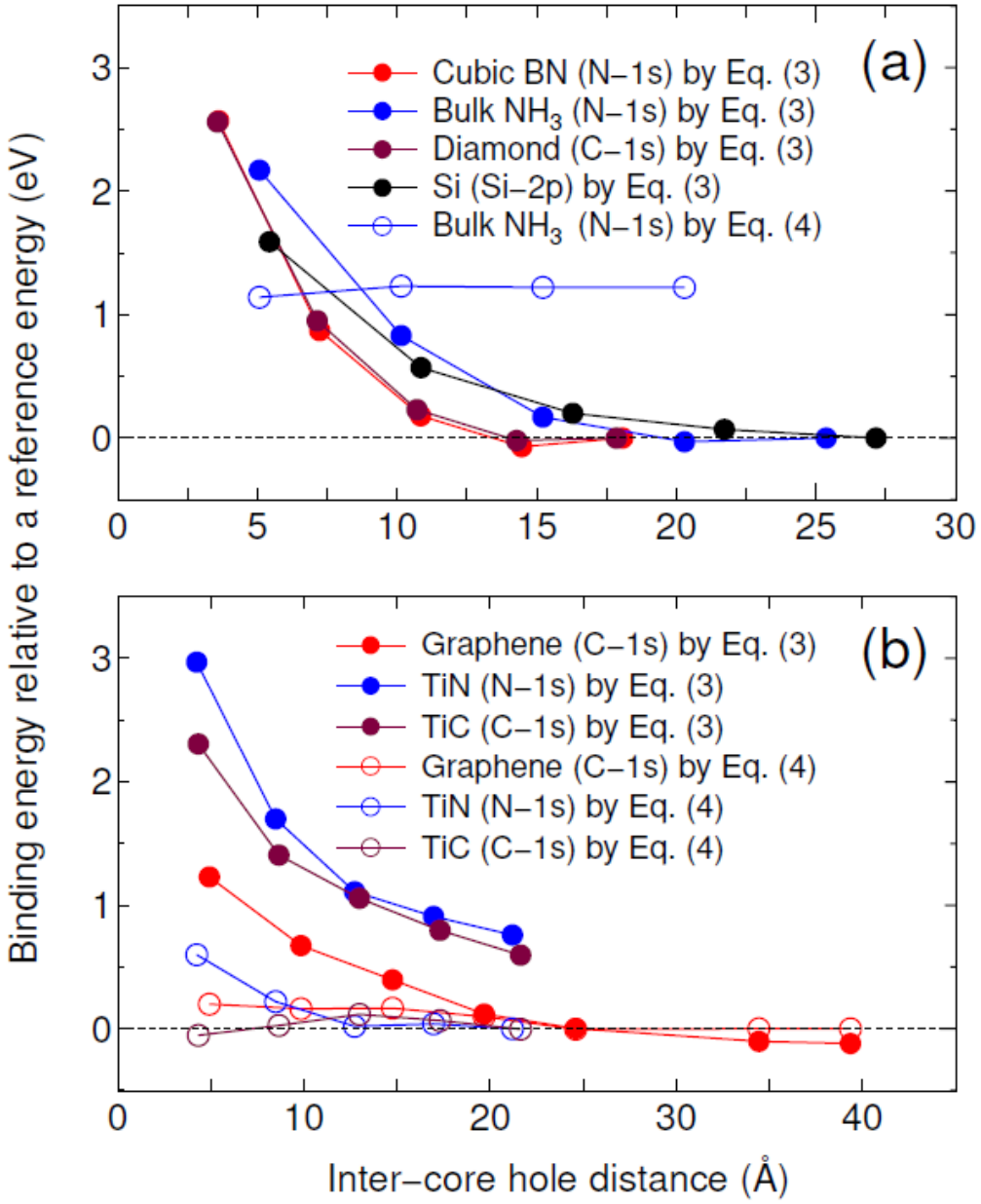

General formula

$$E_b = E_f^{(0)}(N-1) - E_i^{(0)}(N) + \mu_0$$

・・・(3)

For metals

$$E_b = E_f^{(0)}(N) - E_i^{(0)}(N)$$

・・・(4)

- Convergence is attainable around 15～20Å.
- The formula for metals is not applicable for gapped systems.
- Very fast convergence by Eq. (4) for metals.

Difference charge induced by a core hole in Si

- The effective radius is about 7Å.
- The core hole is almost screened on the same Si atom.

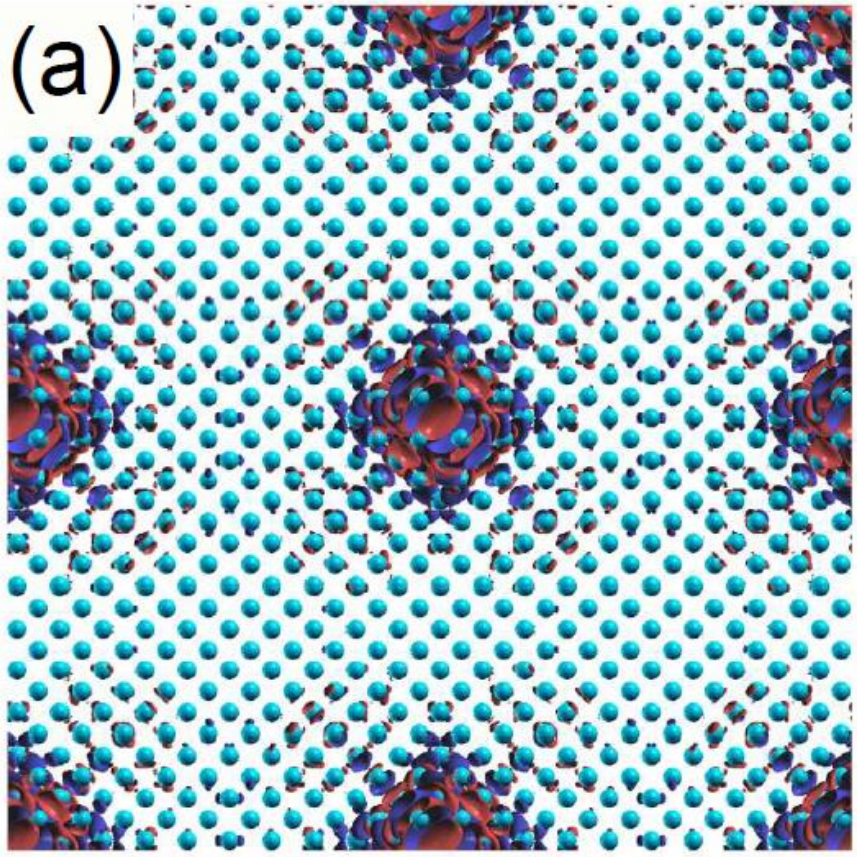

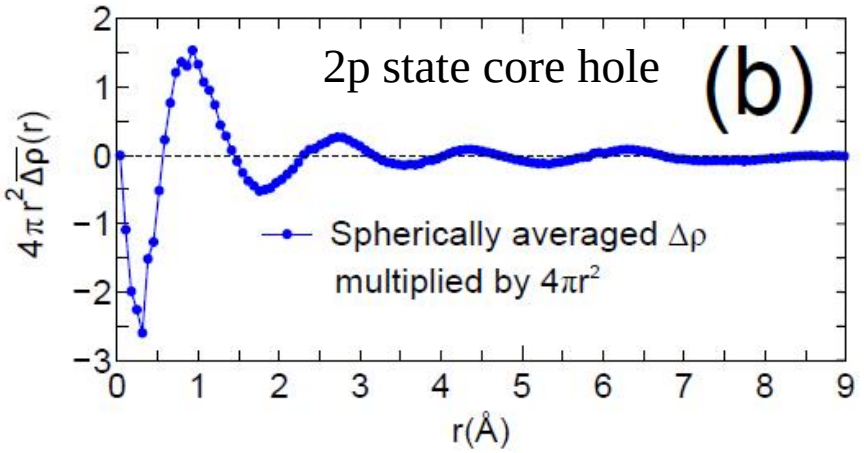

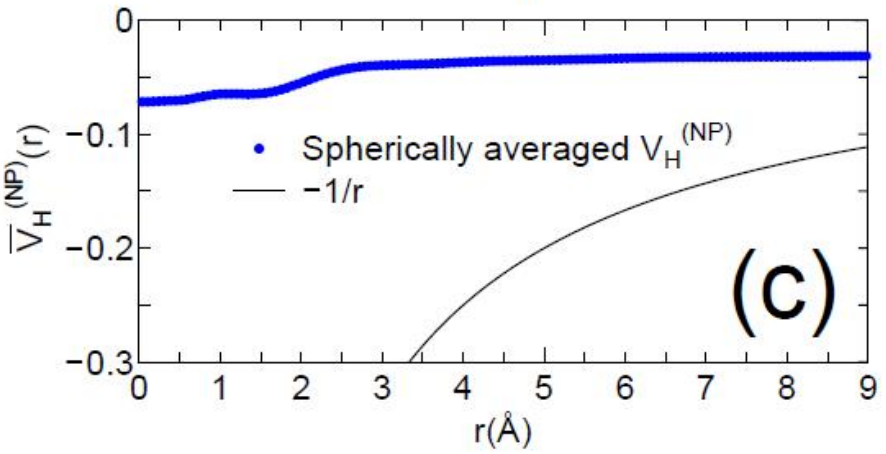

Expt. vs. Calcs. for solids and molecules

Mean absolute error: 0.42 eV/system

Solid	State	Calc. (eV)	Expt. (eV)	Molecule	State	Calc. (eV)	Expt. (eV)
Gapped system				CO	C-1s	295.87	296.19[4)]
c-BN	N-1s	398.87	398.1[4)]	C_2H_2	C-1s	291.24	291.17[4)]
bulk NH_3	N-1s	398.92	399.0[4)]	CO_2	C-1s	296.89	297.66[4)]
Diamond	C-1s	286.50	285.6[4)]	HCN	C-1s	293.35	293.50[4)]
Si	Si-2$p_{1/2}$	100.13	99.8[4)]	N_2	N-1s	409.89	409.83[4)]
Si	Si-2$p_{3/2}$	99.40	99.2[4)]	NH_3	N-1s	404.70	405.60[4)]
(Semi-)Metal				N_2H_4	N-1s	404.82	406.1[4)]
Graphene	C-1s	284.23	284.4[4)]	CO	O-1s	542.50	542.4[4)]
TiN	N-1s	396.43	397.1[4)]	CO_2	O-1s	541.08	541.2[4)]
TiC	C-1s	281.43	281.5[4)]	O_2	O-1s (S=$\frac{1}{2}$)	543.15	544.2[4)]
ZrB_2	B-1s	187.75	187.81[12)]	O_2	O-1s (S=$\frac{3}{2}$)	542.64	543.1[4)]
Hexagonal BN	B-1s	190.19	190.3[13)]	H_2O	O-1s	539.18	539.9[4)]
Pt	Pt-4$f_{7/2}$	71.14	71.10[14)]	SiH_4	Si-2p	106.56	107.3[4)]
Pt	Pt-4$f_{5/2}$	74.53	74.40[14)]	SiF_4	Si-2p	111.02	111.7[4)]

T. Ozaki and C.-C. Lee, Phys. Rev. Lett. 118, 026401 (2017).

Collaboration between experiments and simulations in identification of silicene

Experiments

Prof. Yukiko Yamada-Takamura

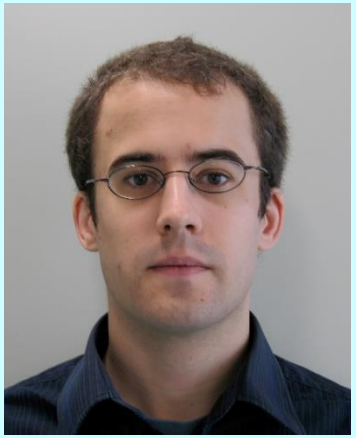

Dr. Antoine Fleurence

Dr. Rainer Friedlein

Prof. Jun Yoshinobu

Simulations

Taisuke Ozaki

Dr. Chi-Cheng Lee

Experimental report of silicene

on $ZrB_2(0001)$

Yamada-Takamura group of JAIST

ZrB_2 on Si(111) is a promising substrate for a photo emitting device of GaN due to the lattice matching, metallicity, and flatness. It was found that Si atoms form a super structure during CVD by probably migration and segregation of Si atoms from the Si substrate.

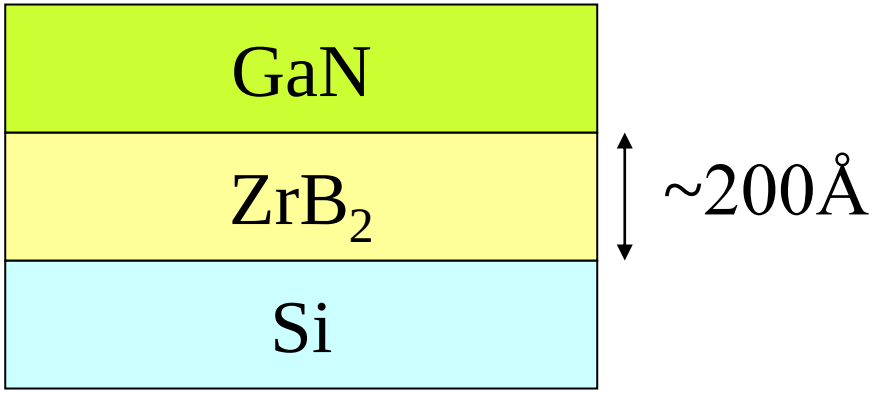

STM image

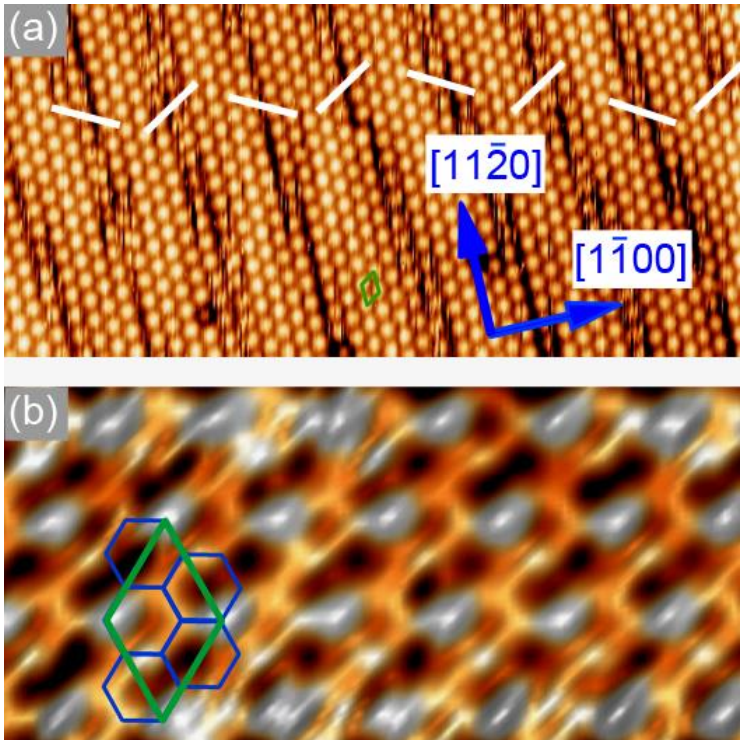

GaN(0001): a= 3.189Å

ZrB_2(0001): a= 3.187Å

A. Fleurence et al., PRL 108, 245501 (2012).

Band dispersion of ZrB_2

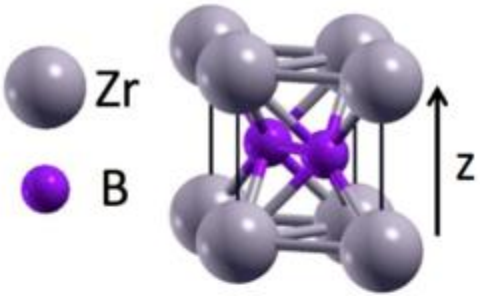

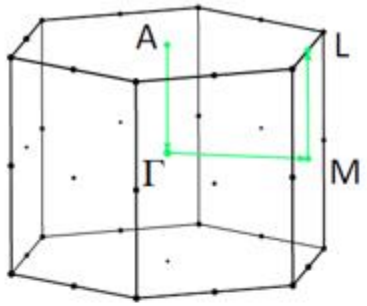

Black: Total
Red: Outermost Zr-d

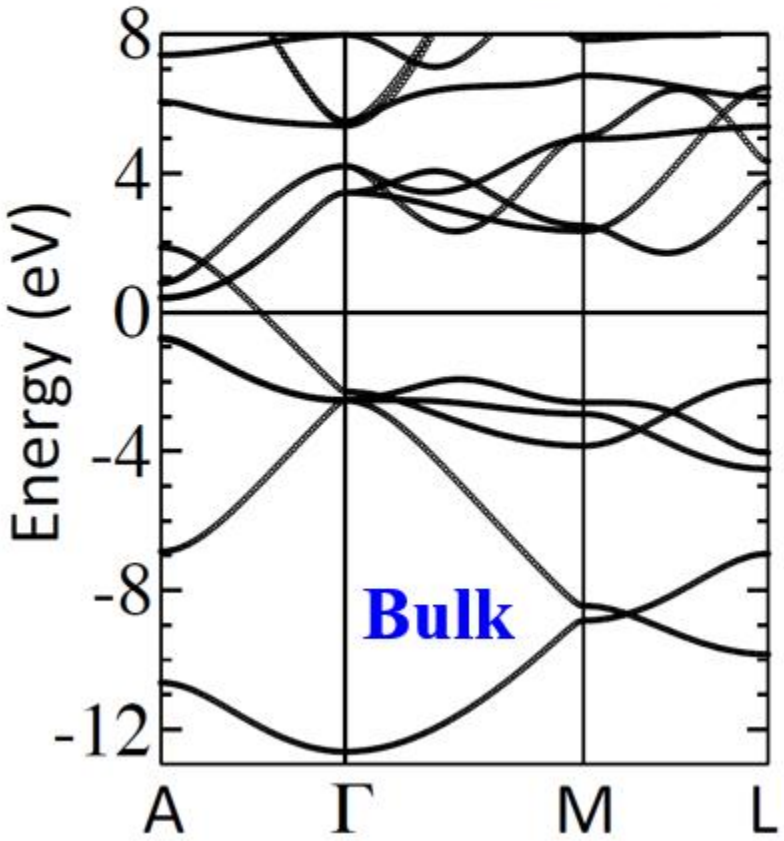

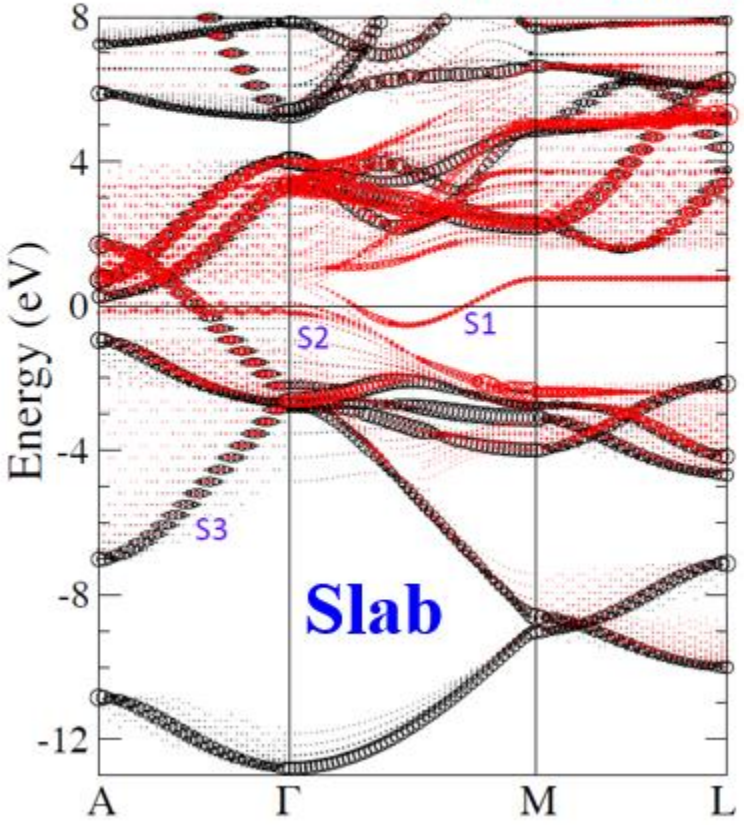

Interaction of a Si atom with the ZrB_2 (0001) surface

On-top

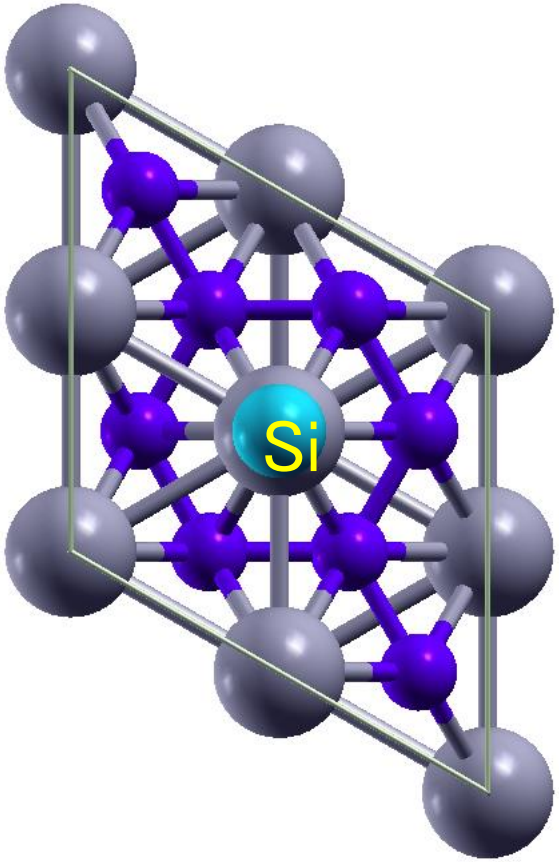

$E_{binding}$= 5.05 eV

Hollow

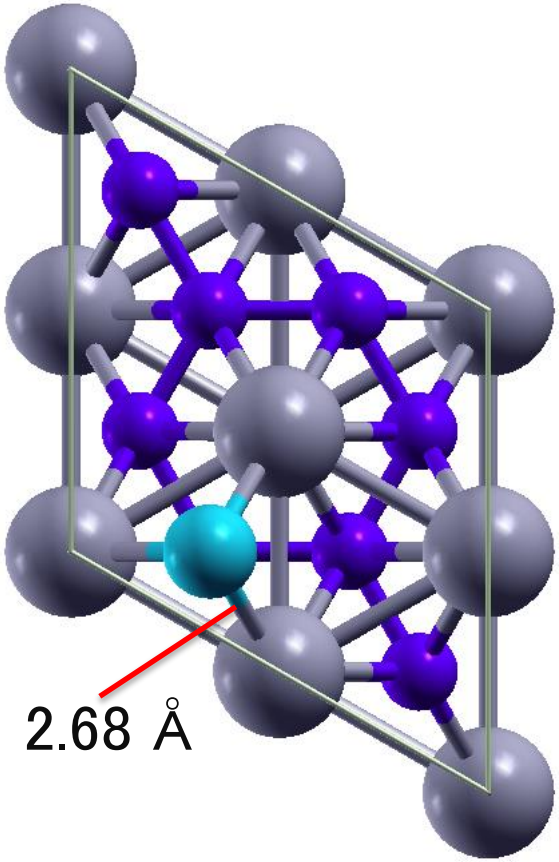

$E_{binding}$= 6.08 eV

Bridge

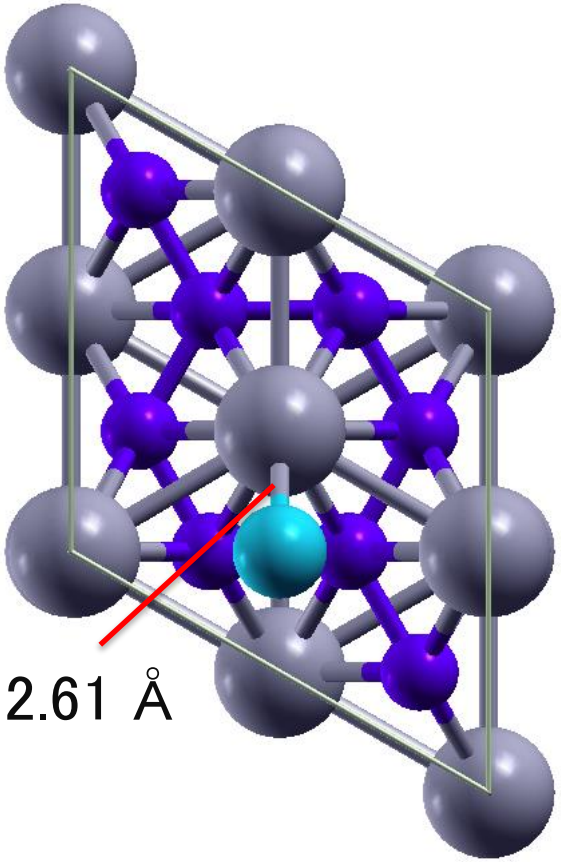

$E_{binding}$= 5.79 eV

Top view of optimized structures

- Two buckled structures are obtained.
- Both the structures keep the honeycomb lattice.

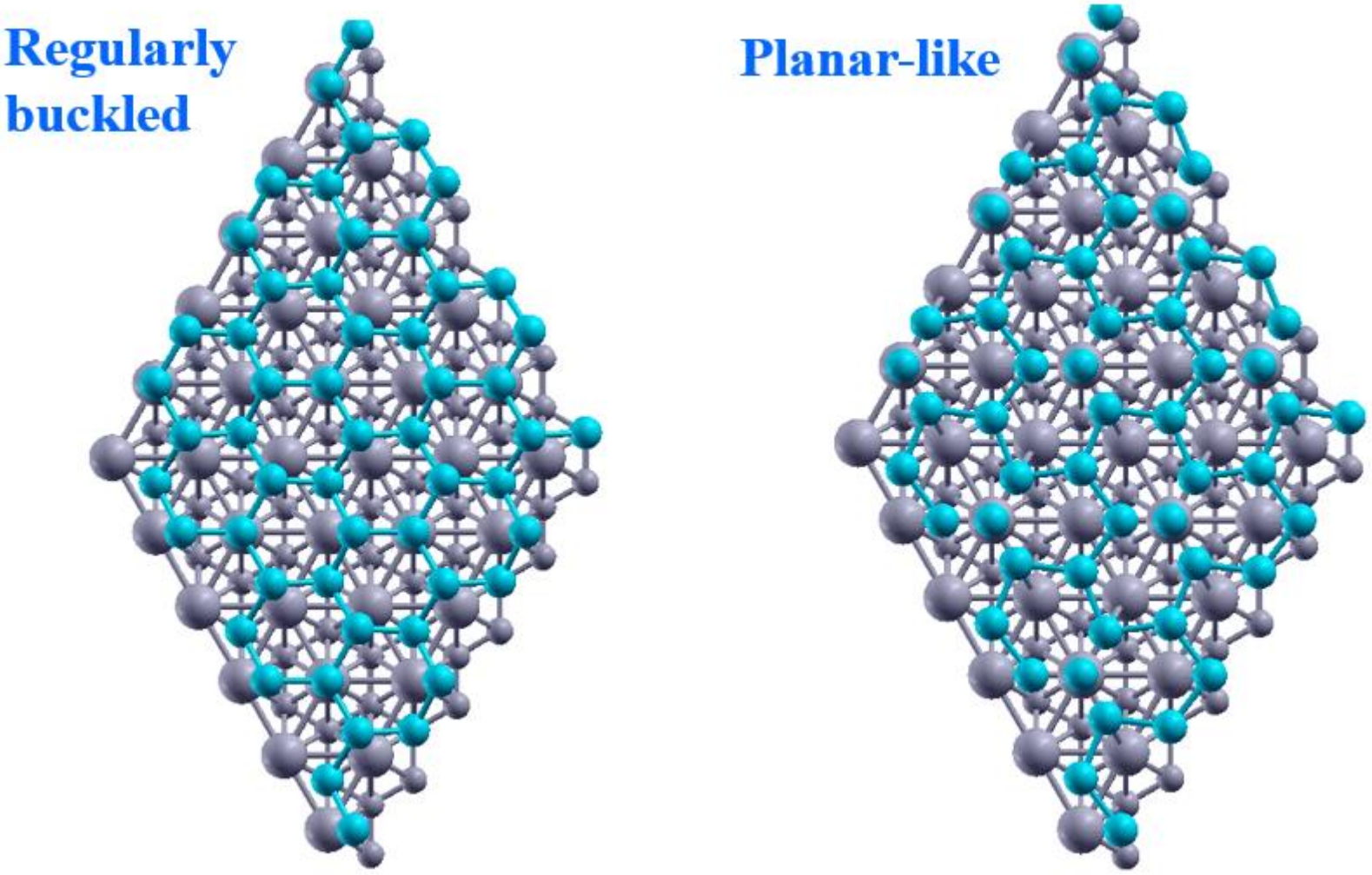

Side view of optimized structures

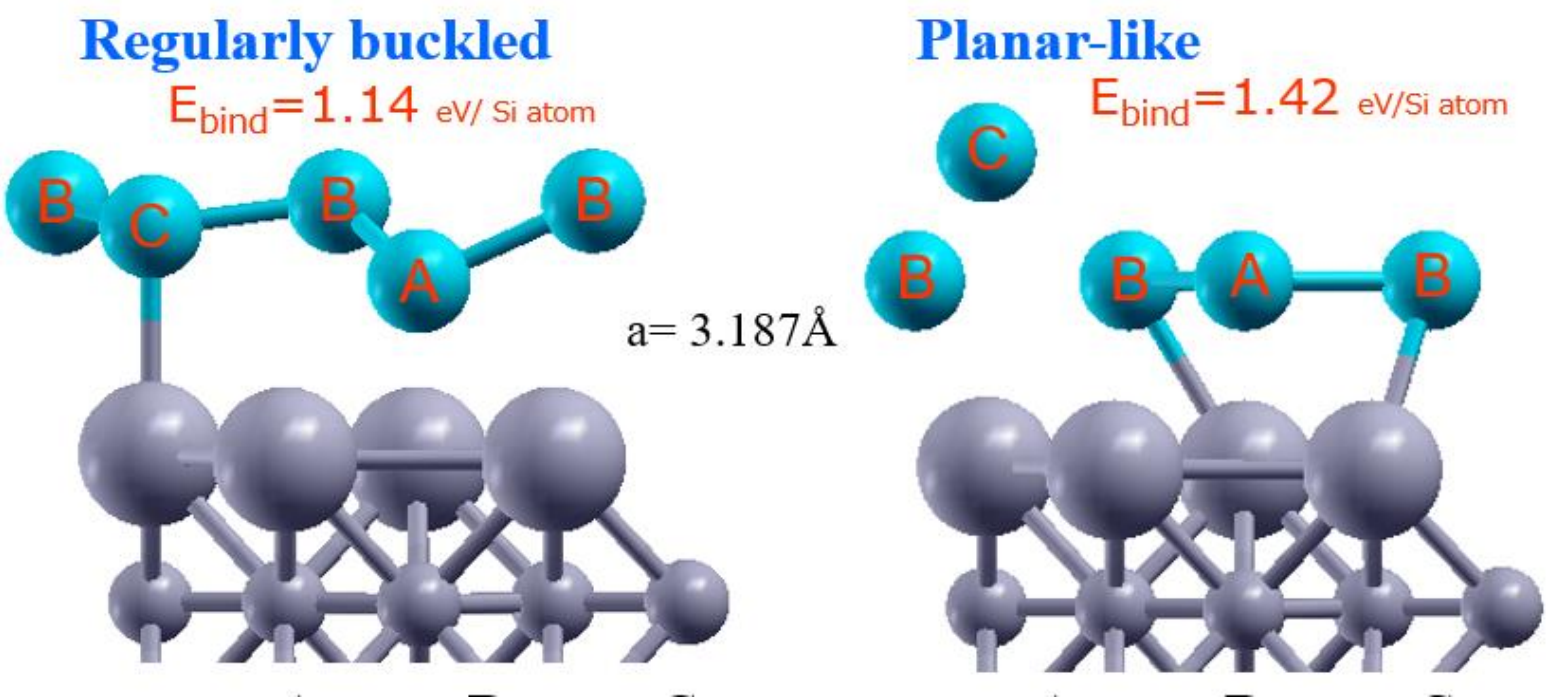

	A	B	C	A	B	C
	hollow	bridge	on-top	hollow	bridge	on-top
Distance from the top Zr layer (Ang.)	2.105	3.043	2.749	2.328	2.331	3.911
Distance with neighbor Si atoms (Ang.)	2.263	2.268	2.249	2.324	2.340	2.380
Angle with neighbor Si atoms (Deg.)	104.2	110.1	118.2	120.2	113.0	80.5

Energy barrier between two structures

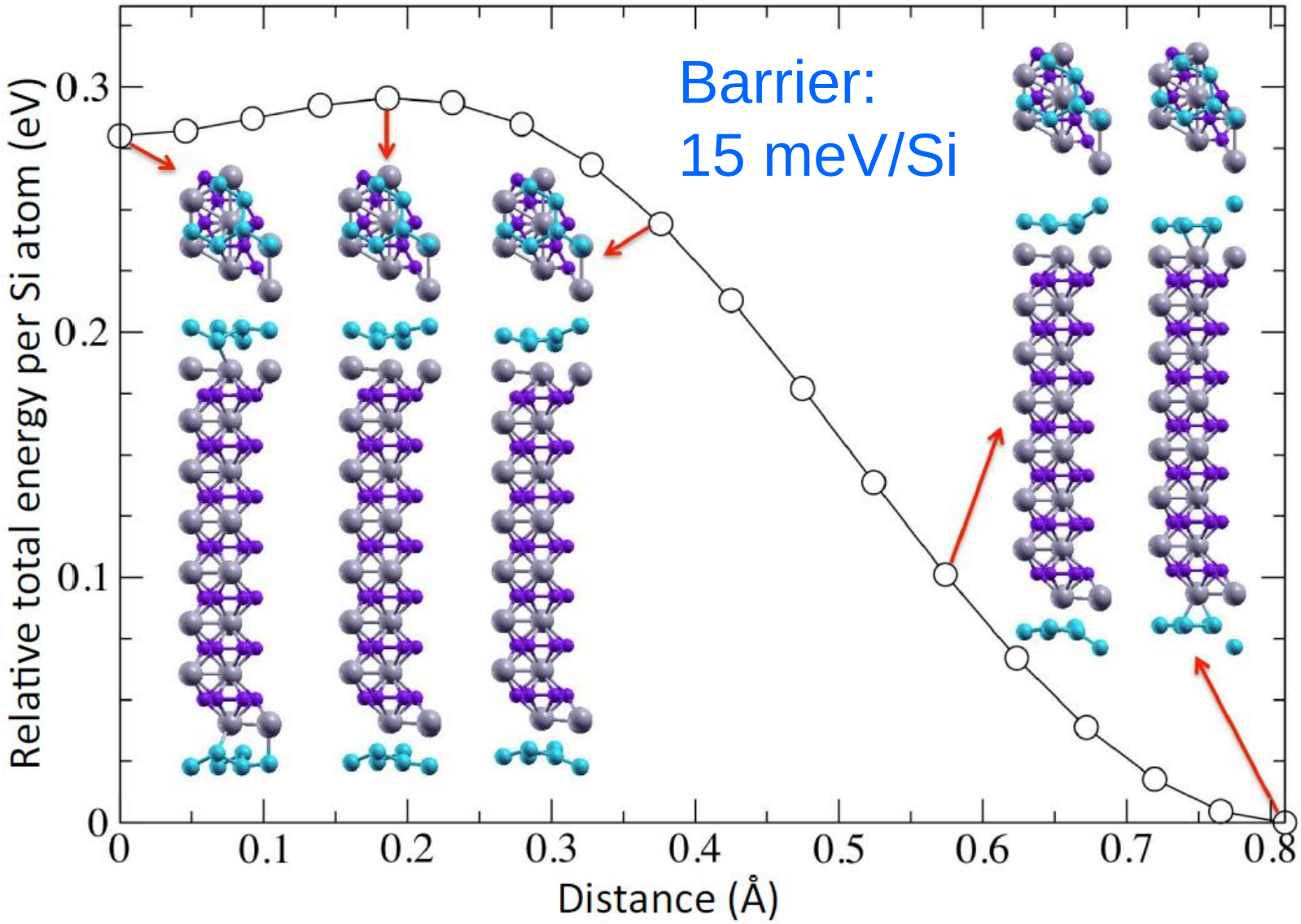

ARPES and calculated bands

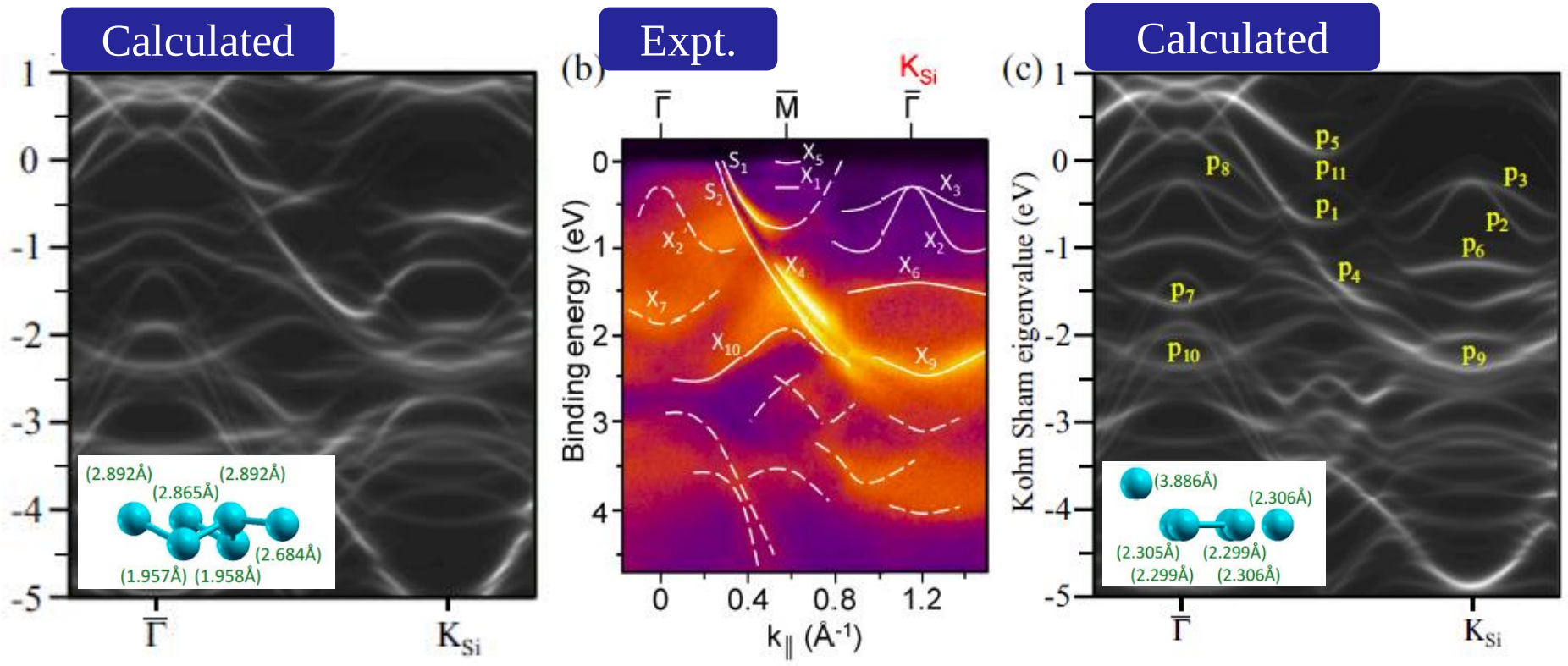

The ARPES intensity spectrum is well reproduced by the band structure of planar-like structure more than that of the buckled like structure, especially for S_1, S_2, X_2 and X_3 bands.

C.-C. Lee et al., PRB **90**, 075422 (2014).

XPS of Si-2p: Expt. vs. calculations

The XPS data is well compared with the calculated binding energy of planar-like structure.

By the Yoshinobu-lab. in ISSP

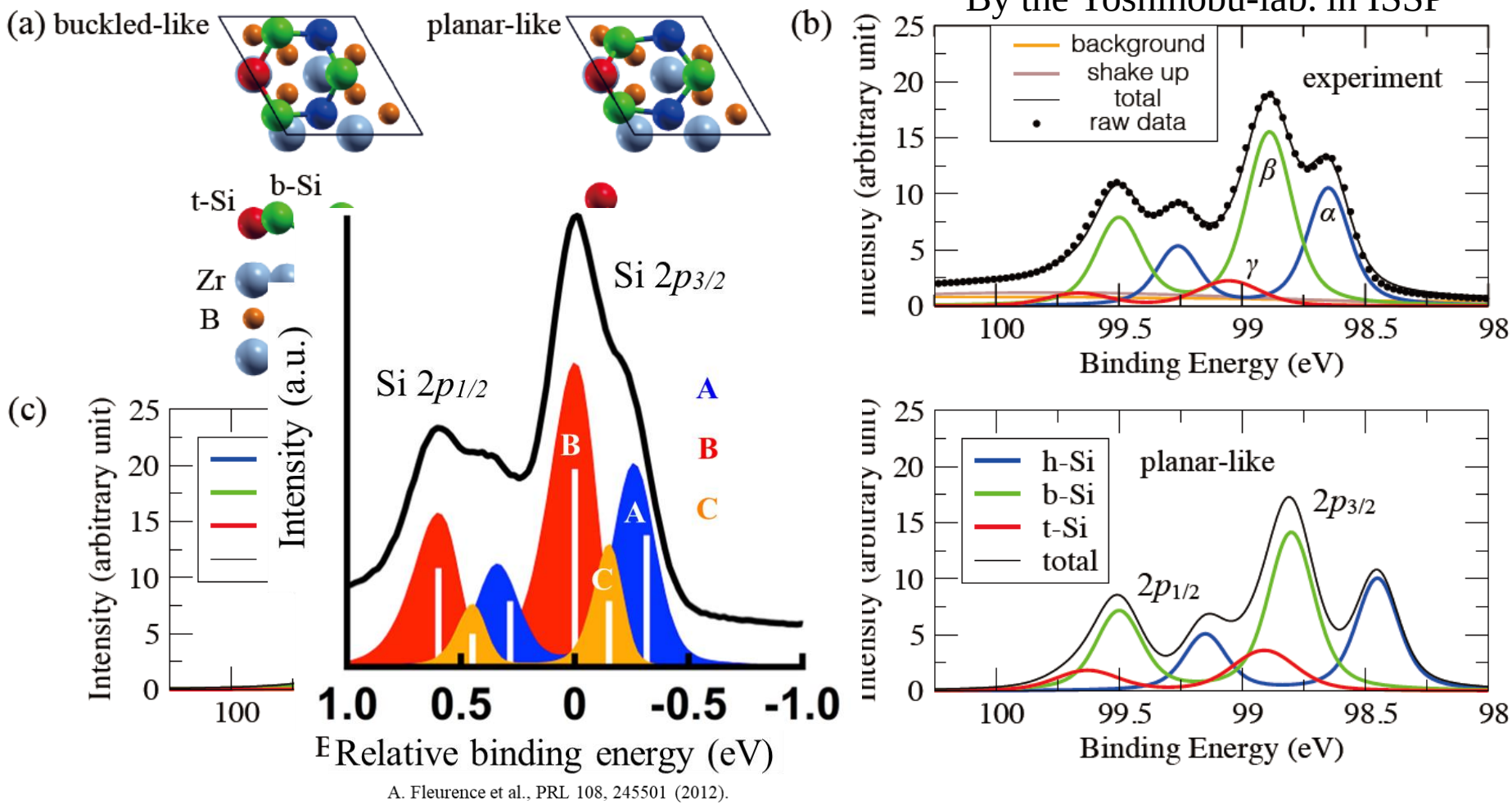

A. Fleurence et al., PRL 108, 245501 (2012).

C.-C. Lee et al., PRB 95, 115437 (2017).

Characterization of structure by expt. and calcs.

In the early speculation, a regularly-buckled structure was supposed.

The DFT calculations of ARPES, phonon, and **XPS** strongly support a planar structure. We now concluded that the experimental structure is the planar one.

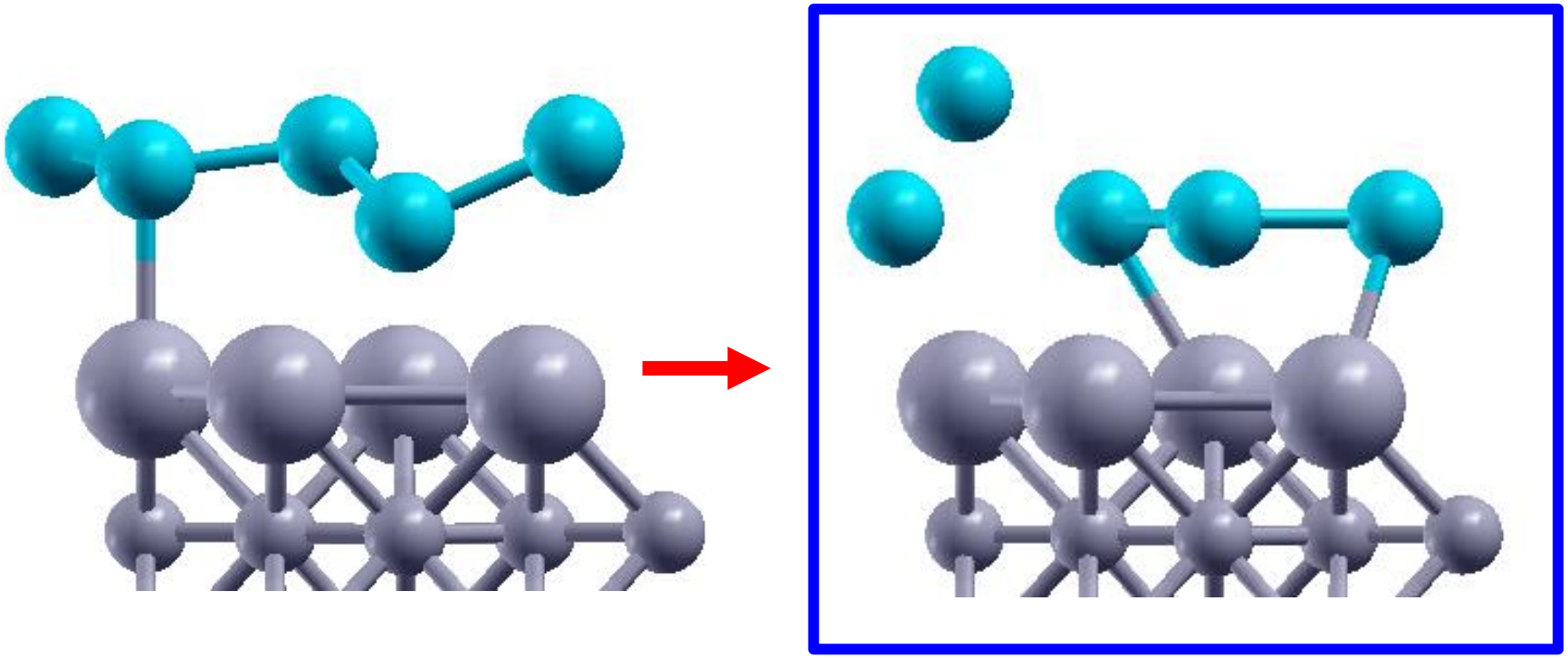

Flat band with bi-triangular lattice

The two-dimensional structure spontaneously generated on a ZrB2 substrate forming a double-triangular lattice was identified through joint experimental (Yukiko Takamura Lab., JAIST, and Yoshinobu Lab., ISSP) and theoretical studies.

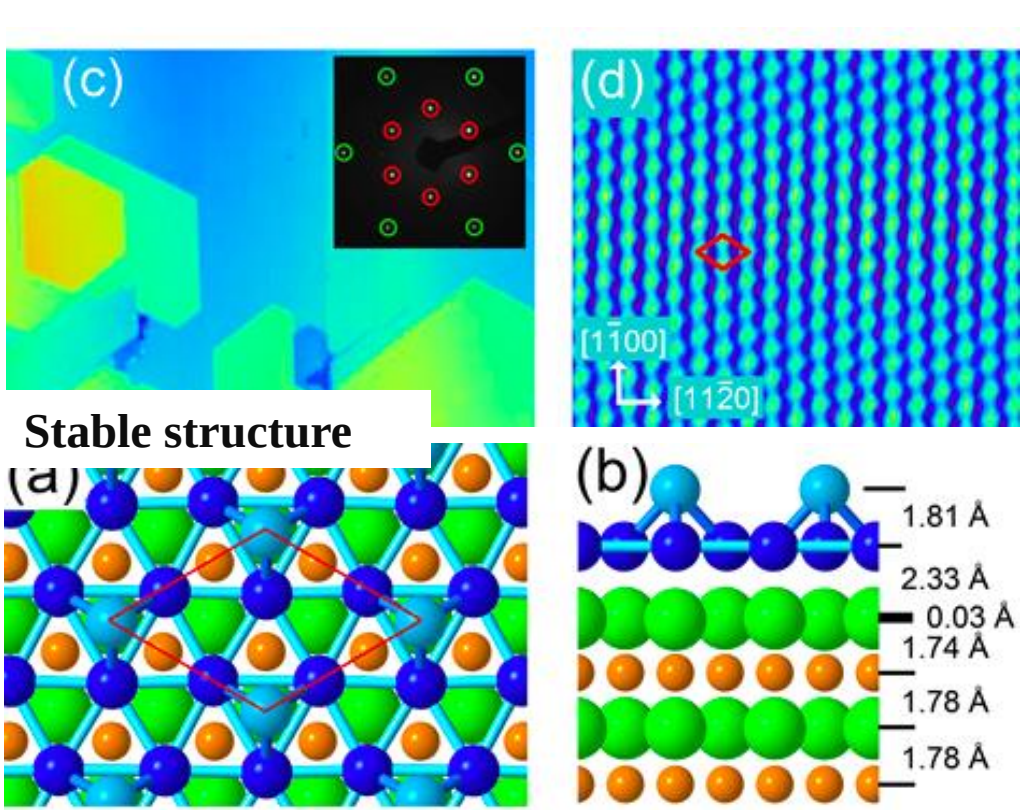

Bi-triangular lattice by Ge

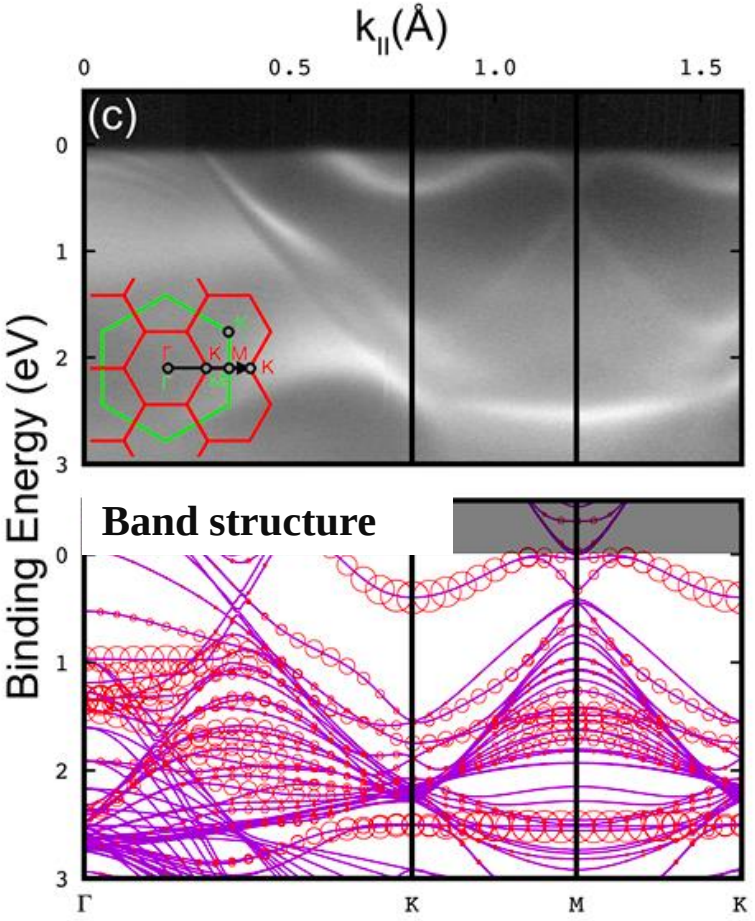

A. Fleurence et al., Phys. Rev. B 102, 201102 (2020).

Why are the band structures of the bi-triangular lattice and Kagome lattice similar?

Starting from the Kagome lattice, a site is added to the lattice. In this case, the bi-triangular lattice can have a Kagome-derived flat band if the following condition holds for the hopping integral.

$$t_2(\epsilon_D - \lambda)/t_3 = t_3$$
$$\lambda = \epsilon_A - t_2 - 2t_1$$

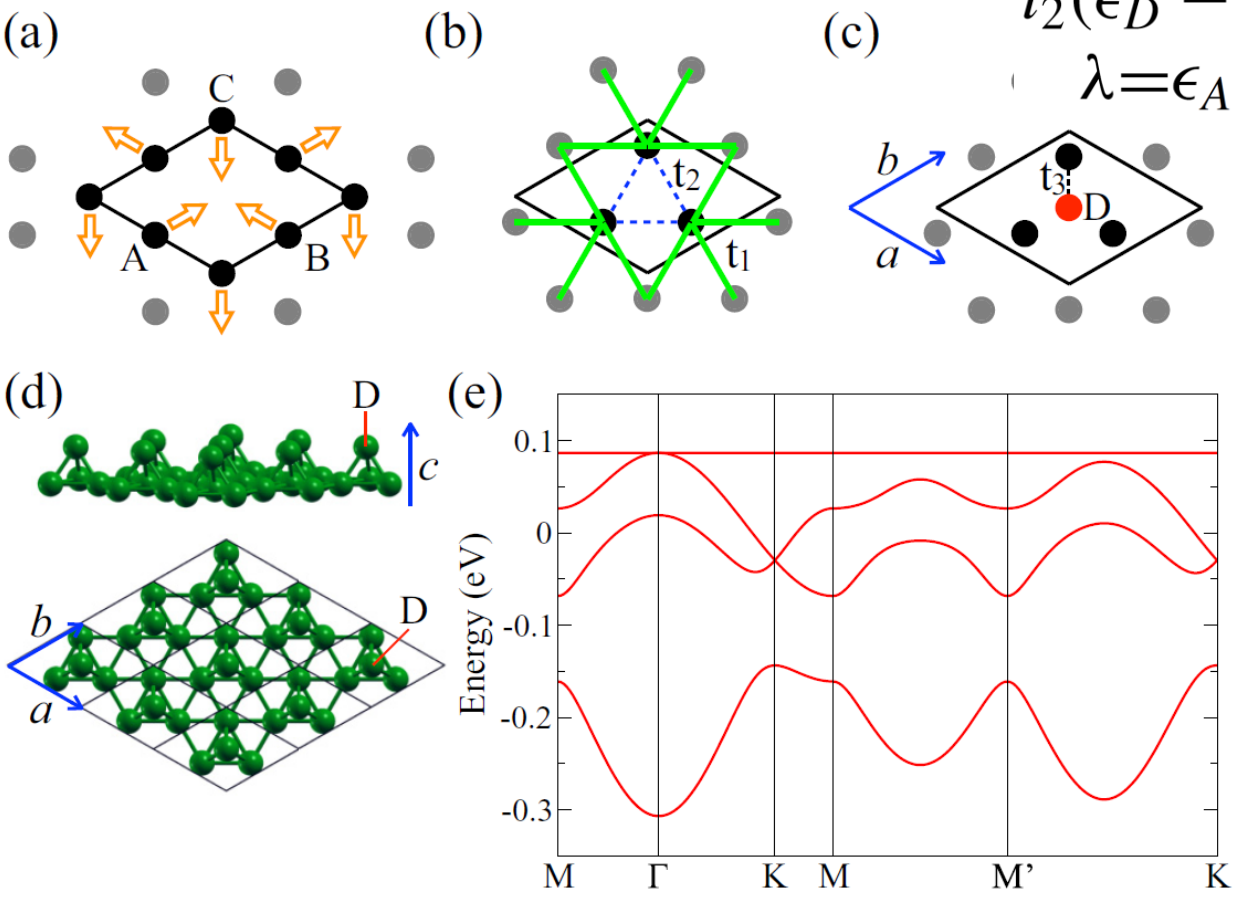

C.C.-Lee et al, Phys. Rev. B 100, 045150 (2019)
Ogata et al., Phys. Rev. B **103**, 205119 (2021).

Borophene in the β_{12} structure on Ag (111)

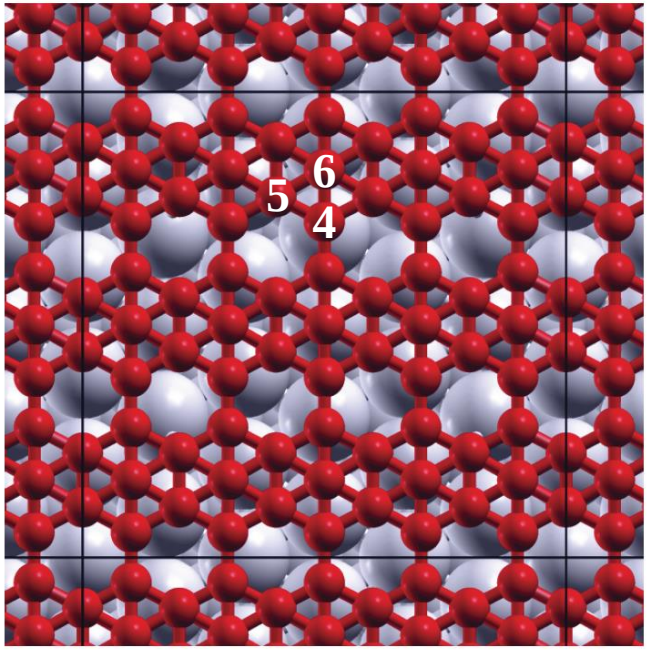

B-1s binding energies

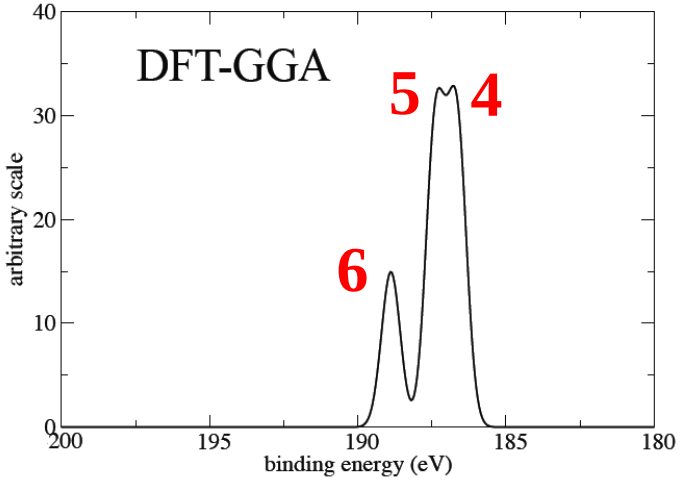

STM images from Feng et al, PRB 94, 041408 (3016).

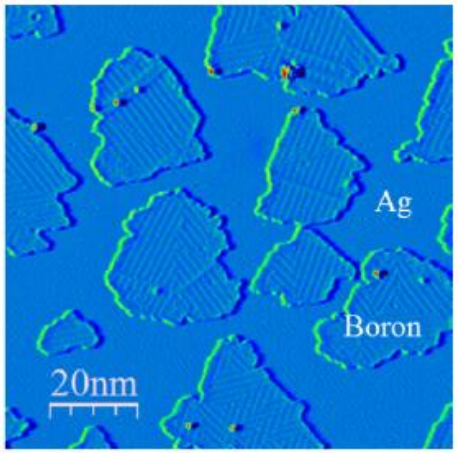

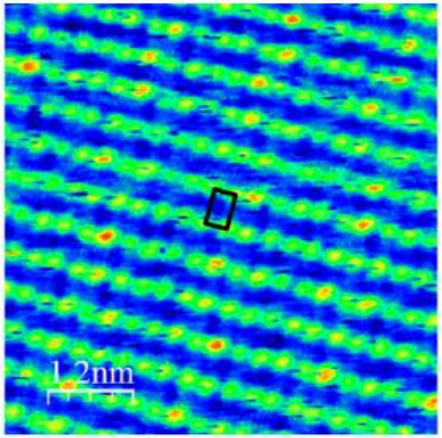

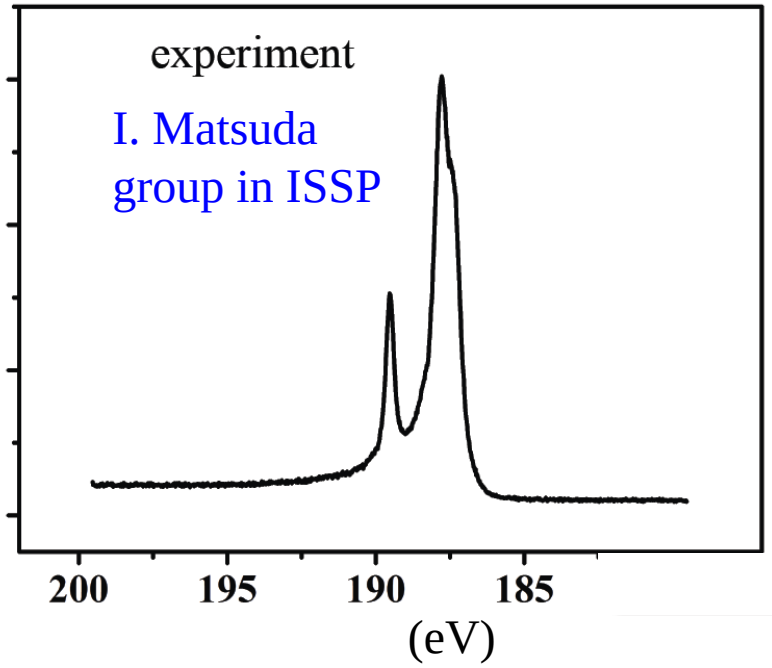

Bonding state in borophene

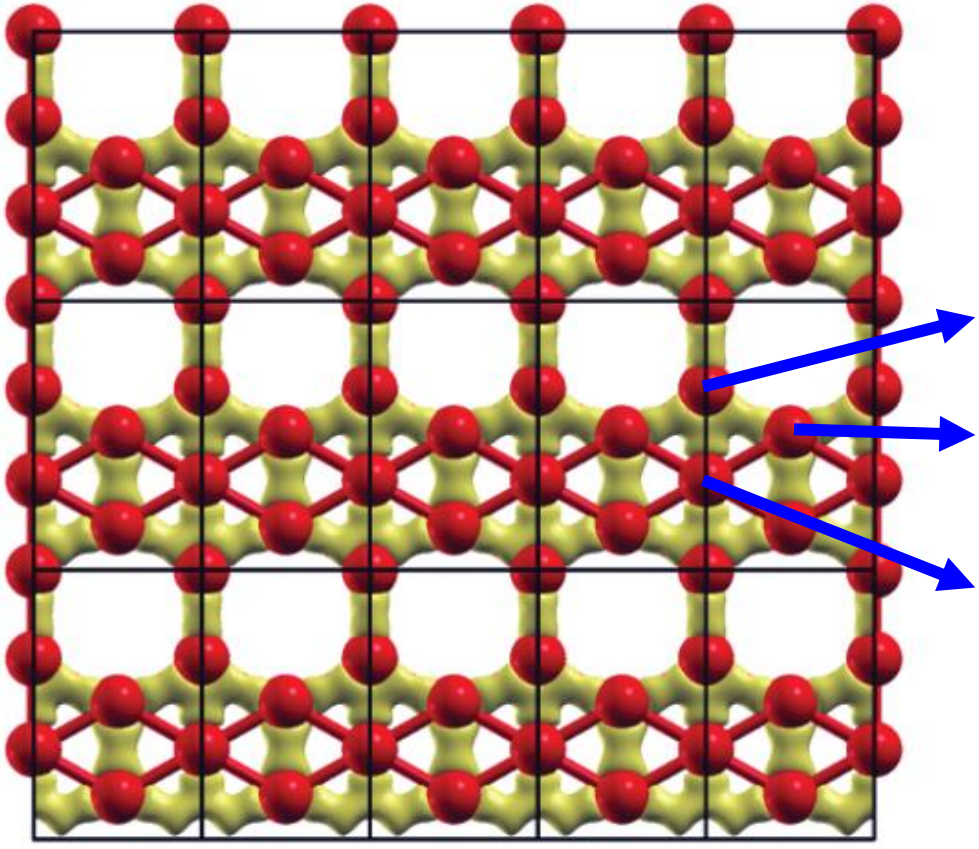

0.125 e/bohr^3

E_b	Coordination number	bonding
186.228 eV	4	4
186.946 eV	5	3
188.646 eV	6	2

The number of coordination and the number of bonds are in an opposite relationship.

C.C. Lee et al., Phys. Rev. B 97, 075430 (2018)

Wannier functions of borophene

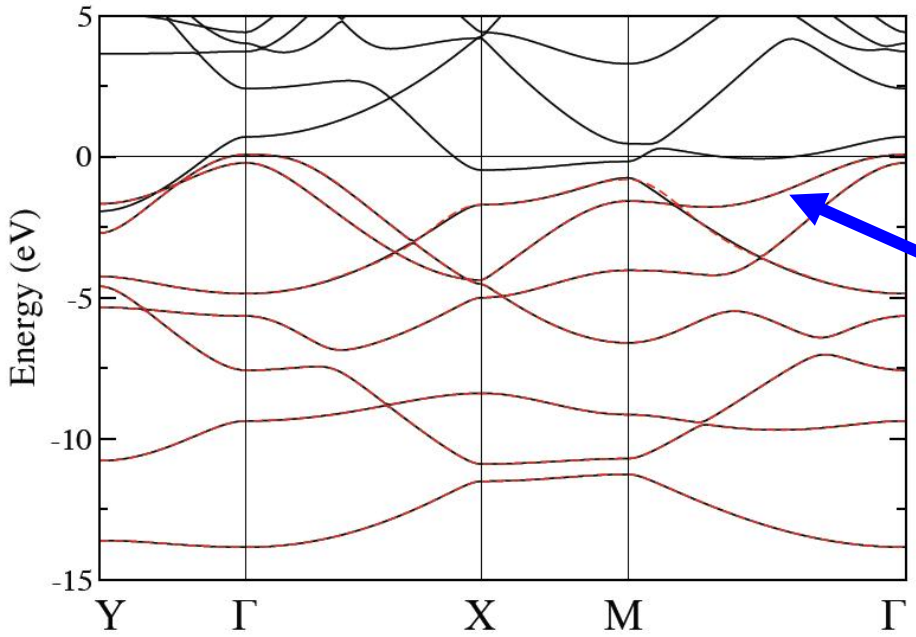

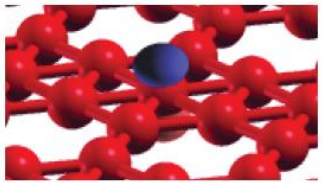

0.1 sqrt(e/bohr^3)

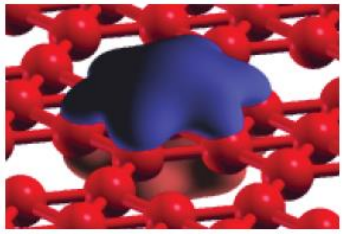

0.05 sqrt(e/bohr^3)

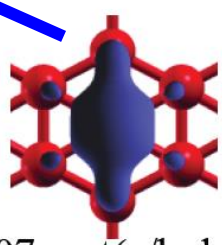

0.07 sqrt(e/bohr^3)

0.23 sqrt(e/bohr^3)

Triangular: donor
Honeycomb: acceptor

XANES:

X-ray Absorption Near Edge Structure

Four types of electronic excitations

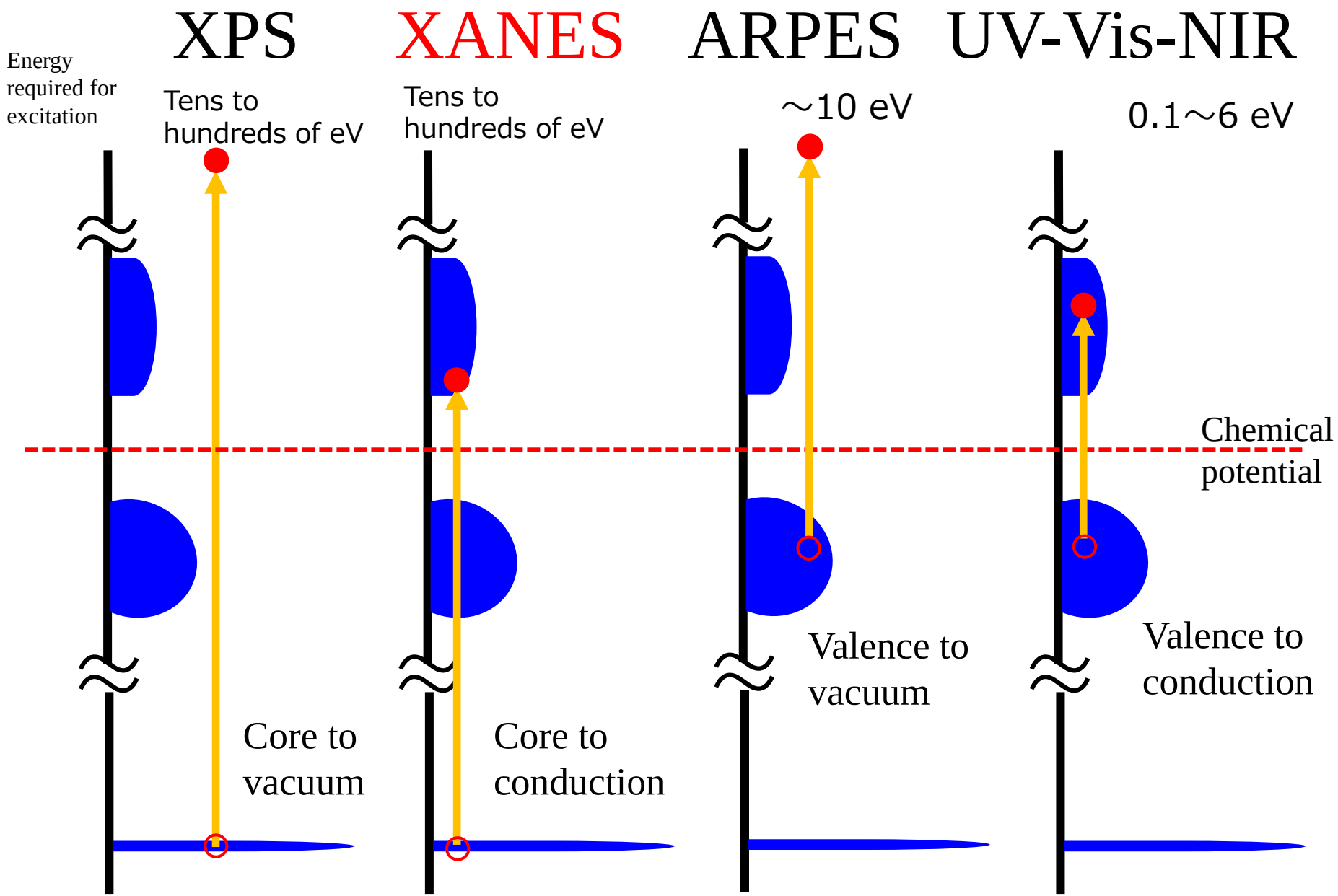

XANES: X-ray Absorption Near Edge Structure

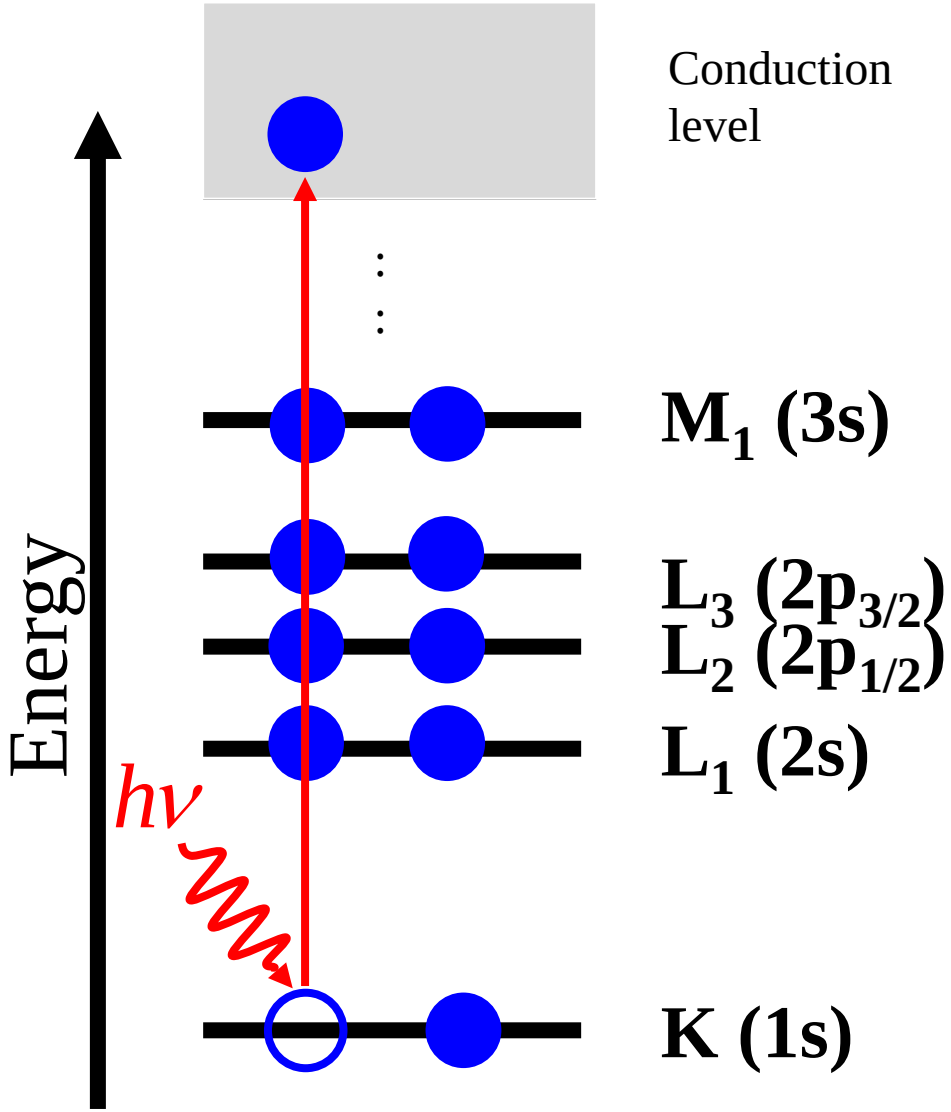

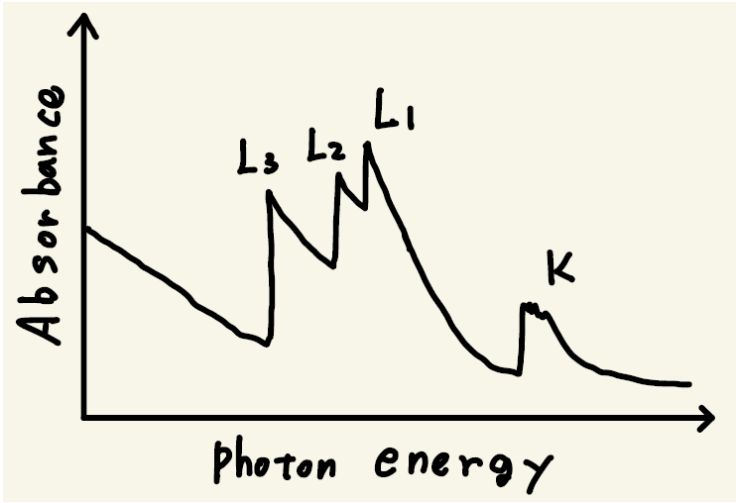

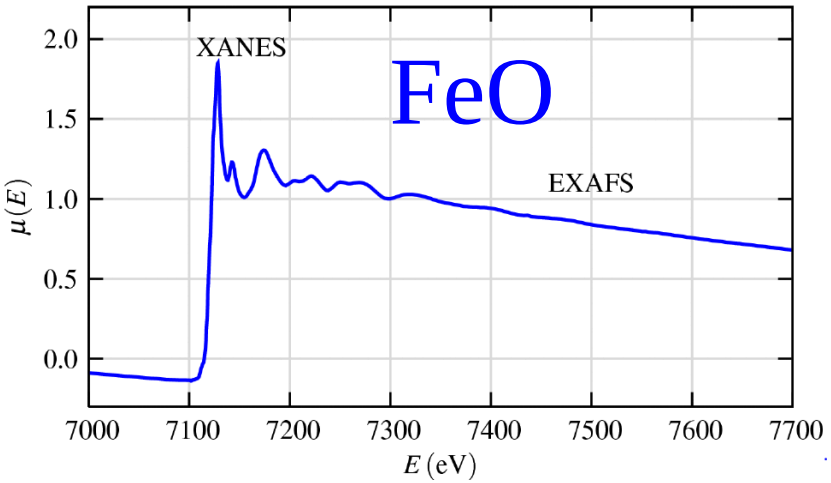

Fundamentals of XAFS
Matthew Newville

The first excited energies and higher

As already discussed for XPS, the total energy E_1 of the first excited state with a core hole can be calculated accurately by solving the following KS eq. with conditions: ΔS=0 and the same number of electron N:

$$\left(\hat{T} + V_{\text{eff}} + \hat{P}\right) | \varphi_{\mu}^{(\mathbf{k})} \rangle = \varepsilon_{\mu}^{(\mathbf{k})} | \varphi_{\mu}^{(\mathbf{k})} \rangle$$

The excitation energies for higher excited states are approximately calculated by

$$\Delta E_k = E_1 + (\varepsilon_{HOMO+k}^{\sigma} - \varepsilon_{LUMO}^{\sigma}) - E_{\text{G}}$$

To ensure ΔS=0 required by the selection rule, σ is chosen to be the same as the core state that we introduced the core hole.

Oscillator strength #1

The simplest treatment of the oscillator strength f is to use the core orbital of the ground state and a valence KS orbital of the final state. Then, based on the Fermi golden rule, one has

$$f_{\mathrm{G,E}} \propto \frac{1}{\omega_{\mathrm{G,E}}} \left| \left\langle \varphi_{\mathrm{c}}^{(\mathrm{G})} \left| \hat{P} \right| \varphi_{\mathrm{v}}^{(\mathrm{E})} \right\rangle \right|^2 \qquad \omega_{\mathrm{G,E}} = \frac{\left| E_{\mathrm{G}} - E_{\mathrm{E}} \right|}{\hbar}$$

Another method which might be more accurate is to employ the Slater KS determinants of the ground and excited states.

$$f_{\mathrm{G,E}} \propto \frac{1}{\omega_{\mathrm{G,E}}} \left| \left\langle \Phi_{\mathrm{G}} \left| \hat{P} \right| \Phi_{\mathrm{E}} \right\rangle \right|^2$$

M. Takahashi, Phys. Rev. B 78, 155108 (2008).
Y. Liang et al., Phys. Rev. Lett. 118, 096402 (2017).

The rigorous justification for the treatment is still an open question. At this moment, we would like to see how it works.

Oscillator strength #2

Since Φ_I and Φ_J are not orthogonal each other, the momentum matrix elements are calculated as explained below.

$$\Phi_I = \frac{1}{\sqrt{N!}} \left| \varphi_{I1} \varphi_{I2} \varphi_{I3} \cdots \varphi_{I(N-1)} \varphi_{IN} \right|$$

We introduce an overlap matrix Z_{IJ} between KS orbitals as

$$Z_{IJ} = \begin{pmatrix} \langle \varphi_{I1} | \\ \langle \varphi_{I2} | \\ \vdots \\ \langle \varphi_{IN} | \end{pmatrix} \left(|\varphi_{J1}\rangle, |\varphi_{J1}\rangle, \cdots, |\varphi_{JN}\rangle \right)$$

Using Z_{IJ}, one can define the dual orbitals as

$$\left(|\tilde{\varphi}^I_{J1}\rangle, |\tilde{\varphi}^I_{J2}\rangle, \cdots, |\tilde{\varphi}^I_{J}\rangle \right) = \left(|\varphi_{J1}\rangle, |\varphi_{J1}\rangle, \cdots, |\varphi_{JN}\rangle \right) \left(Z_{IJ} \right)^{-1}$$

Then, we have the following bi-orthogonality:

$$\langle \varphi_{I\mu} | \tilde{\varphi}^I_{J\nu} \rangle = \delta_{\mu\nu}$$

Oscillator strength #3

Φ_J can be rewritten by Z_{IJ} as

$$\begin{aligned}\Phi_J &= \frac{1}{\sqrt{N!}}\left|\varphi_{J1}\varphi_{J2}\varphi_{J3}\cdots\varphi_{J(N-1)}\varphi_{JN}\right| \\ &= \frac{1}{\sqrt{N!}}\left|\left(\tilde{\varphi}^I_{J1}\tilde{\varphi}^I_{J2}\tilde{\varphi}^I_{J3}\cdots\tilde{\varphi}^I_{J(N-1)}\tilde{\varphi}^I_{JN}\right)Z_{IJ}\right| \\ &= \frac{1}{\sqrt{N!}}\left|\tilde{\varphi}^I_{J1}\tilde{\varphi}^I_{J2}\tilde{\varphi}^I_{J3}\cdots\tilde{\varphi}^I_{J(N-1)}\tilde{\varphi}^I_{JN}\right|\left|Z_{IJ}\right| = \left|Z_{IJ}\right|\tilde{\Phi}^I_J\end{aligned}$$

Using the formula of Φ_J, the momentum elements can be calculated as

$$\begin{aligned}\left\langle\Phi_I\left|P\right|\Phi_J\right\rangle &= \left|Z_{IJ}\right|\sum_{\mu=1}^{N}\left\langle\varphi_{I\mu}\left|P\right|\tilde{\varphi}^I_{J\mu}\right\rangle, \\ &= \left|Z_{IJ}\right|\mathrm{Tr}\left(C_I^{\dagger}PC_J\left(Z_{IJ}\right)^{-1}\right)\end{aligned}$$

where P is the matrix of momentum operator for basis orbitals defined as

$$P = \begin{pmatrix}\langle\chi_1| \\ \langle\chi_2| \\ \vdots \\ \langle\chi_{N_b}|\end{pmatrix}\hat{p}\left(|\chi_1\rangle,|\chi_2\rangle,\cdots,|\chi_{N_b}\rangle\right)$$

Carbon K edge spectrum in acetylene molecule

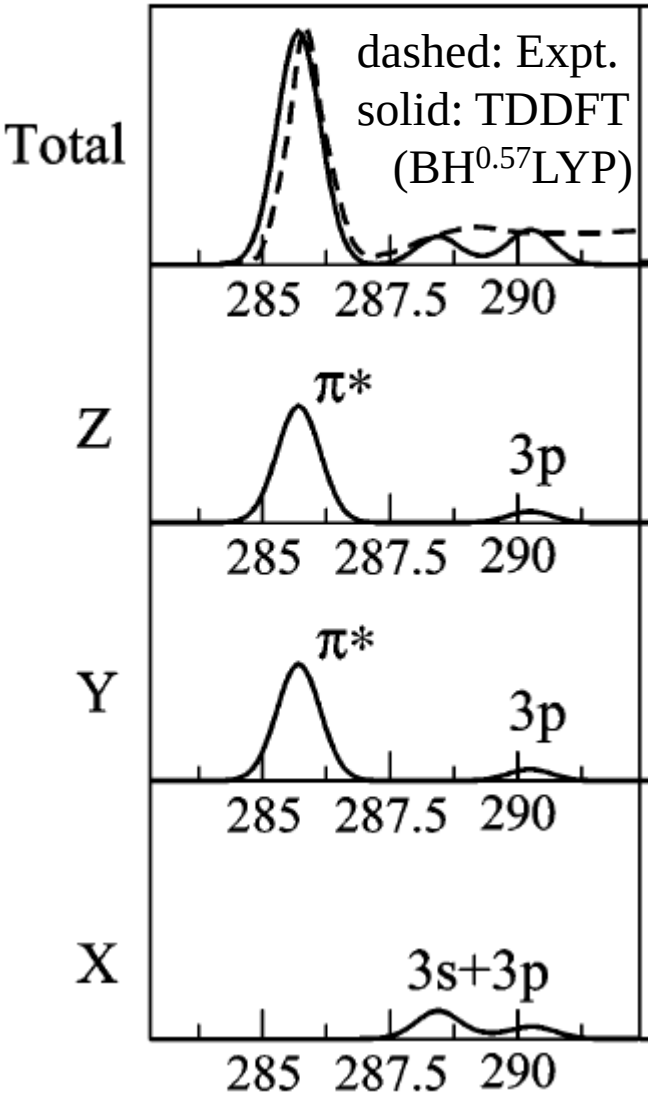

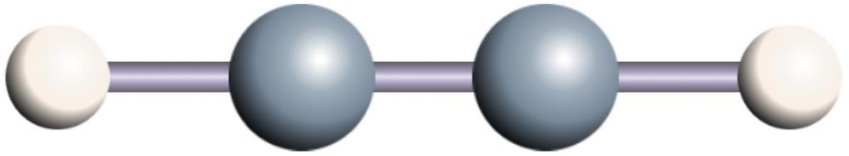

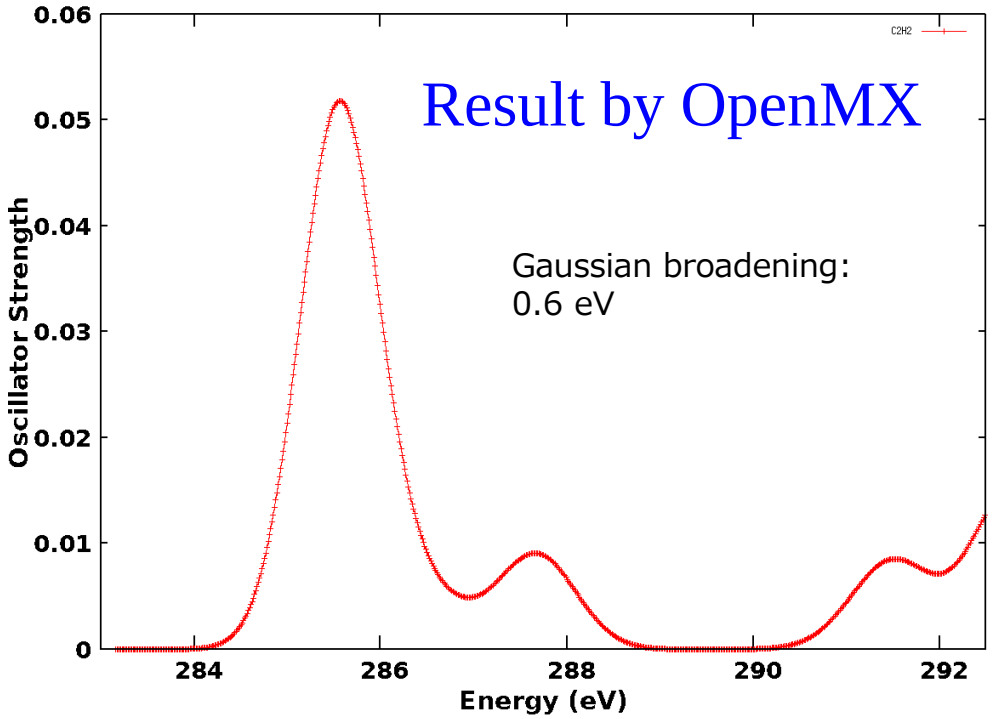

N. A. Besley et al., J. Phys. Chem. C 111, 3333 (2007).

Carbon K edge spectrum in ethylene molecule

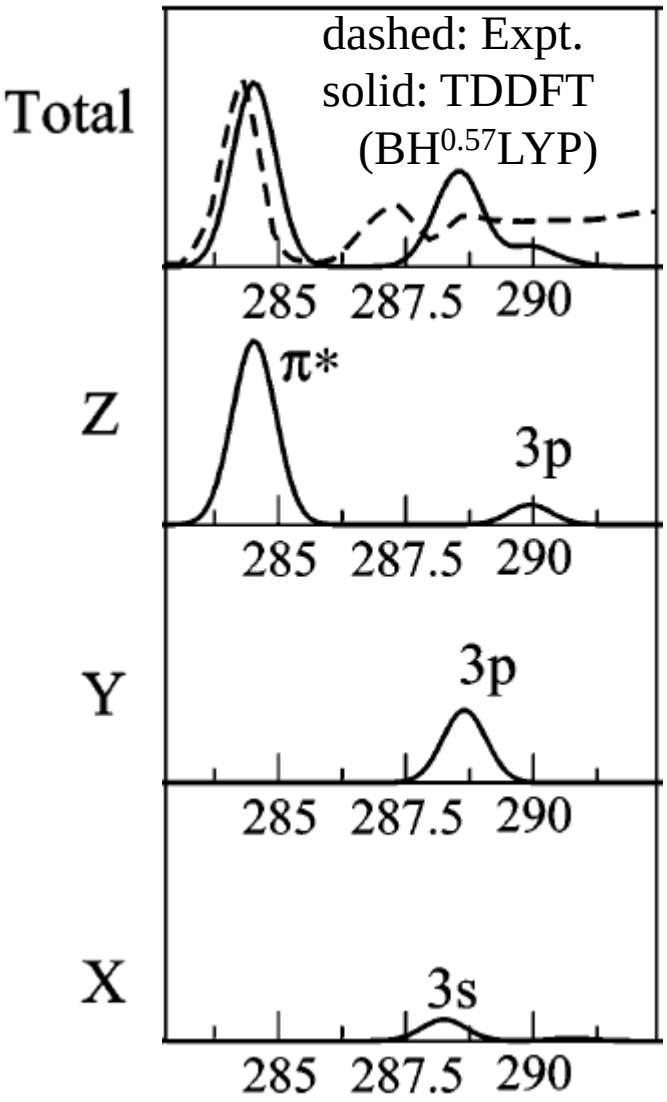

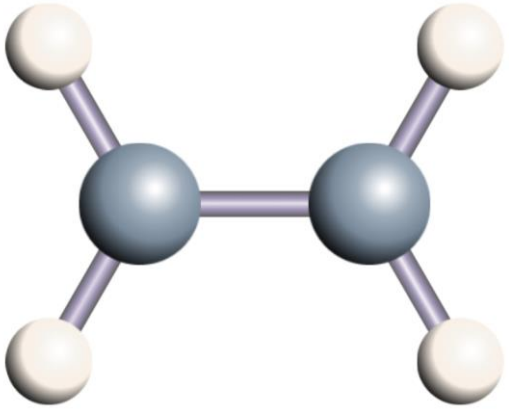

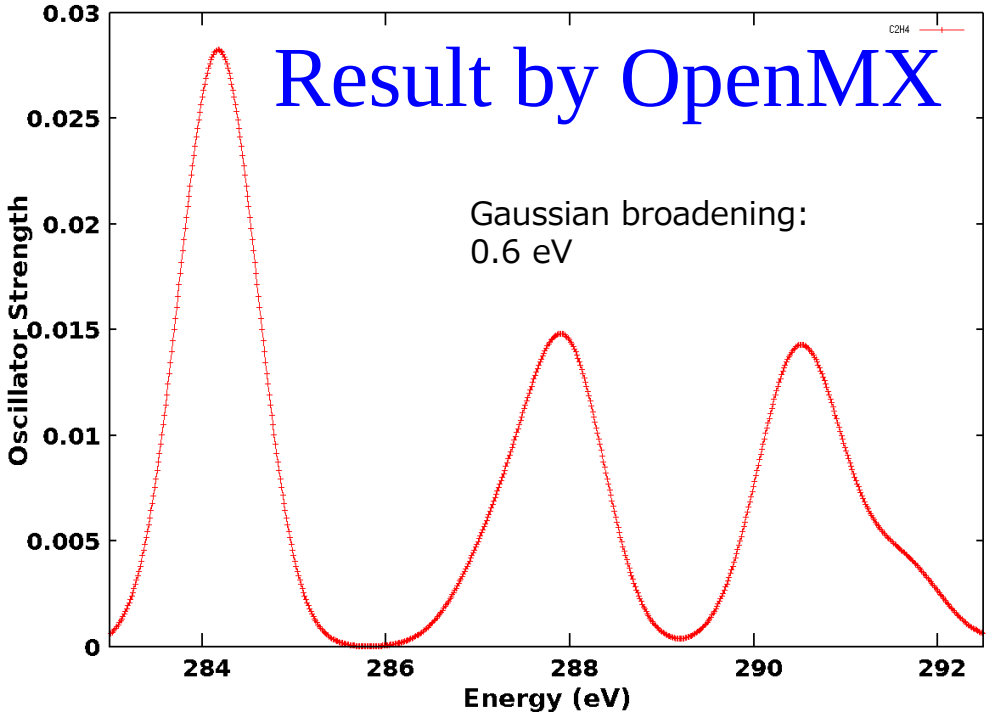

N. A. Besley et al., J. Phys. Chem. C 111, 3333 (2007).

Carbon K edge spectrum in ethane molecule

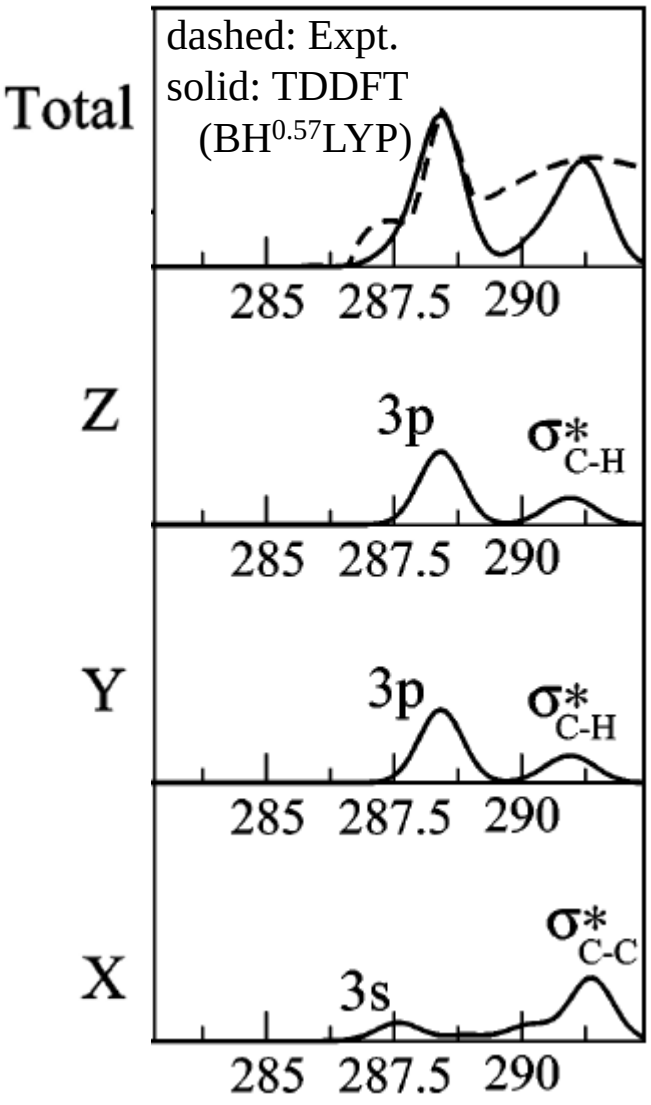

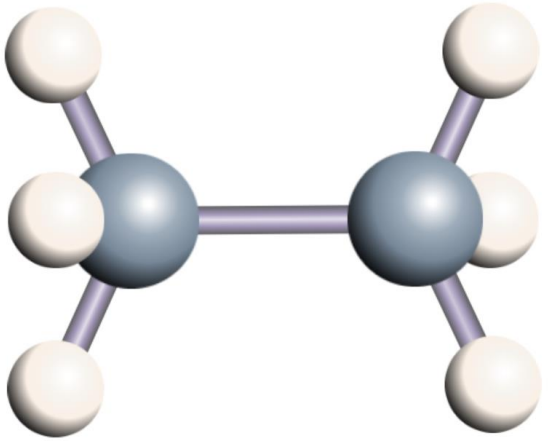

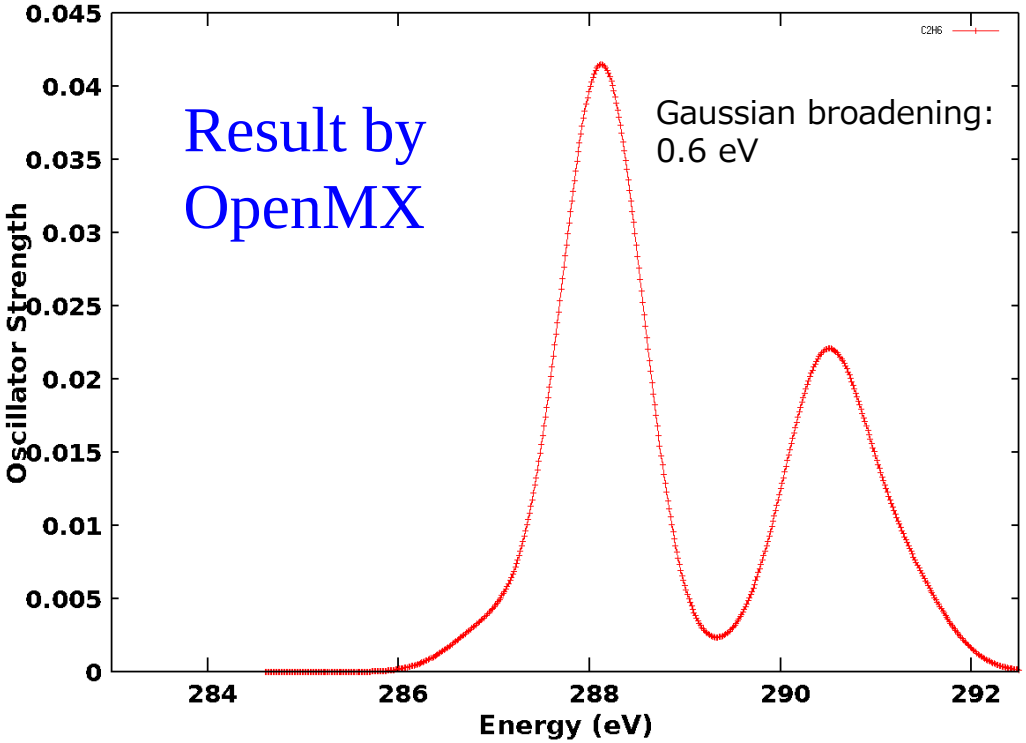

N. A. Besley et al., J. Phys. Chem. C 111, 3333 (2007).

Boron K edge spectrum in cubic BN

Calcs. by FEFF and experiments

B K-XANES for c-BN

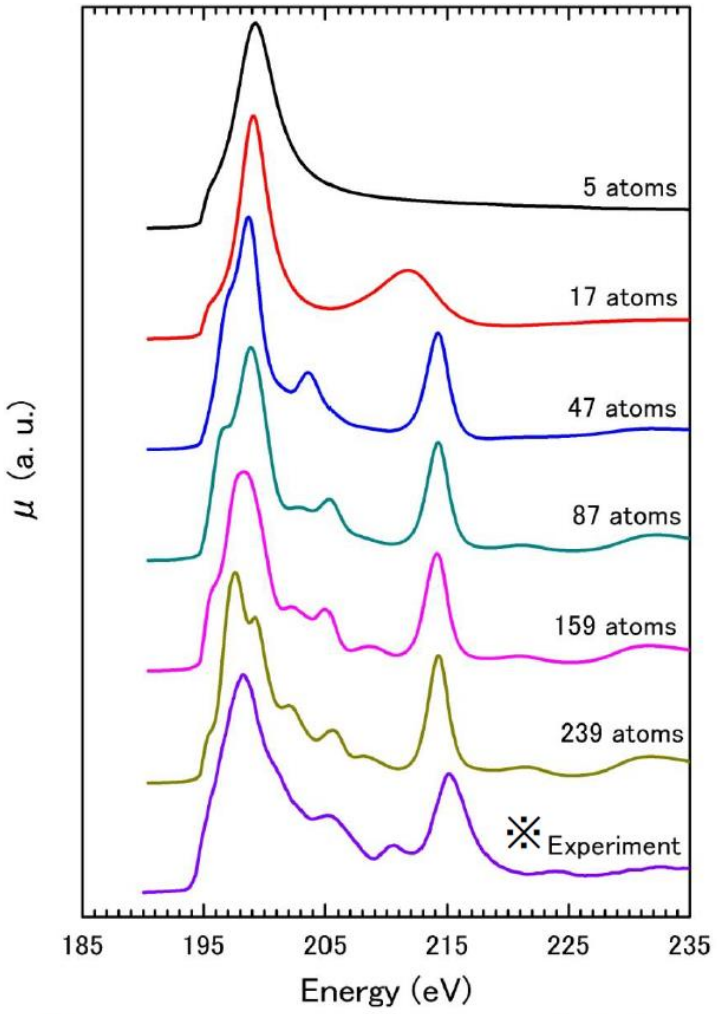

※D. N. Javawardane *et. al.*, Phys. Rev. B **64** (2001) 115107

Result by OpenMX

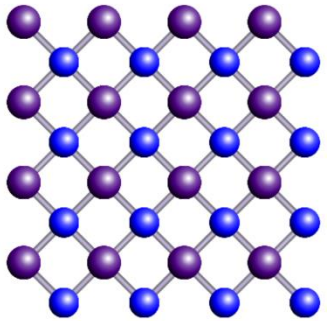

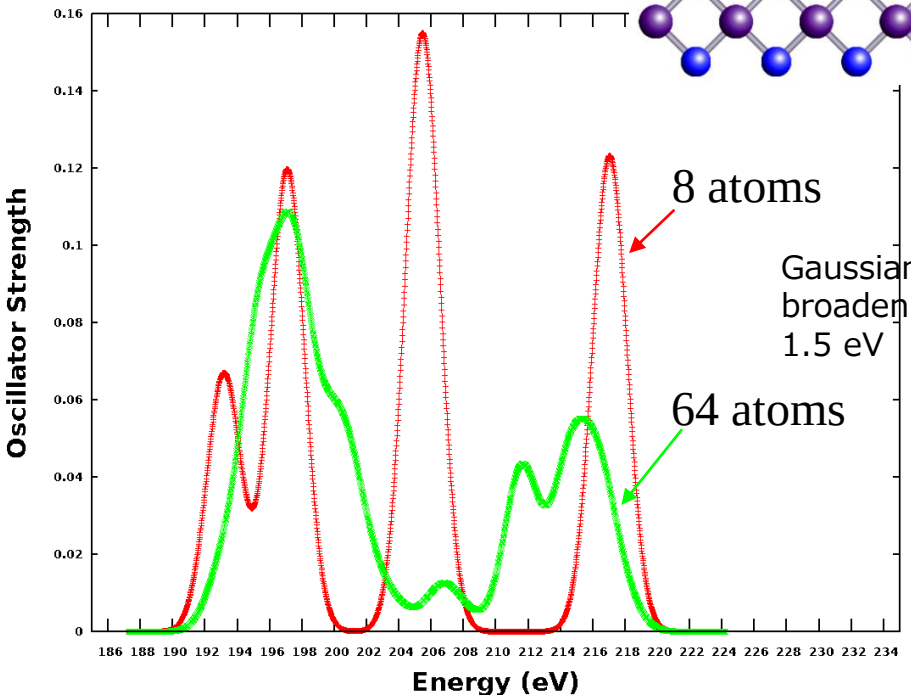

Gaussian broadening: 1.5 eV

The case with 64 atoms is well compared to the experiment.

The lower main peak: Calc. vs Expt.

	Calc.	Expt.
Acetylene (C-K)	285.56	285.8[a]
Ethylene (C-K)	284.17	284.3[a]
Ethane (C-K)	287.00	287.2[a]
c-BN (B-K)	195.28	195.5[b]

in eV

(a) Hitchcock, A. P.; Brion, C. E. J. Electron Spectrosc. Relat. Phenom. 10, 317 (1977).
(b) D. N. Jayawardane et al, Phys. Rev. B **64**, 115107 (2001).

Although the benchmark calculations are still limited, it seems that the accuracy is the same as that for XPS.

Outlook

- A first principles method to calculated absolute binding energies of core level has been introduced based on density functional theory with the following features.

  - applicable to insulators and metals
  - accessible to absolute binding energies
  - screening of core and valence electrons on the same footing
  - SCF treatment of spin-orbit coupling
  - exchange interaction between core and valence states

- The accuracy and general applicability have led to successful collaborations to experiments including silicene, bi-triangular Ge, and borophene.

- The further extensions to XANENS and XMCD spectra seem to be an interesting direction.

Acknowledgments

- Dr. Chi-Cheng Lee (Tamkang Univ.)
- Prof. Yukiko Takamura-Yamada (JAIST)
- Dr. Antoine FLEURENCE (JAIST)
- Dr. Leiner Friedlein (Meyer Burger)
- Prof. Atsushi Yoshinobu (ISSP, Univ. of Tokyo)
- Dr. Kozo Mukai (ISSP, Univ. of Tokyo)
- Prof. Iwao Matsuda (ISSP, Univ. of Tokyo)
- Prof. Marie D‘angelo (Université Pierre et Marie Curie /CNRS)
- Prof. Kazutoshi Gohara (Hokkaido Univ.)
- Dr. Kenji Yamazaki (Hokkaido Univ.)